

Effect of Nonmagnetic Impurity in Nearly Antiferromagnetic Fermi Liquid: Magnetic Correlations and Transport Phenomena

Hiroshi KONTANI and Masanori OHNO¹

¹ Department of Physics, Nagoya University, Furo-cho, Nagoya 464-8602, Japan.

(Dated: July 14, 2018)

In nearly antiferromagnetic (AF) metals such as high- T_c superconductors (HTSC's), a single nonmagnetic impurity frequently causes nontrivial widespread change of the electronic states. To elucidate this long-standing issue, we study a Hubbard model with a strong onsite impurity potential based on an improved fluctuation-exchange (FLEX) approximation, which we call the CV^I -FLEX method. This model corresponds to the HTSC with dilute nonmagnetic impurity concentration. We find that (i) both local and staggered susceptibilities are strongly enhanced around the impurity. By this reason, (ii) the quasiparticle lifetime as well as the local density of states (DOS) are strongly suppressed in a wide area around the impurity (like a Swiss cheese hole), which causes the “huge residual resistivity” beyond the s-wave unitary scattering limit. We stress that the excess quasiparticle damping rate caused by impurities has strong \mathbf{k} -dependence due to non-s-wave scatterings induced by many-body effects, so the structure of the “hot spot/cold spot” in the host system persists against impurity doping. This result could be examined by the ARPES measurements. In addition, (iii) only a few percent of impurities can cause a “Kondo-like” upturn of resistivity ($d\rho/dT < 0$) at low T when the system is very close to the AF quantum critical point (QCP). The results (i)-(iii) obtained in the present study, which cannot be derived by the simple FLEX approximation, naturally explains the main impurity effects in HTSC's. We also discuss the impurity effect in heavy fermion systems and organic superconductors.

PACS numbers: 72.10.-d, 74.81.-g, 74.72.-h, 71.27.+a

I. INTRODUCTION

In strongly correlated electron systems, the presence of nonmagnetic impurities with low concentration can cause drastic changes of electronic properties of the bulk system. Thus, the impurity effect is a useful probe to investigate the electronic states of the host system. In under-doped high- T_c superconductors (HTSC's), nonmagnetic impurities (such as Zn) causes a huge residual resistivity beyond the s-wave unitary scattering limit. Moreover, NMR measurements reveal that both the local and the staggered spin susceptibilities are strongly enhanced around the impurity. Until now, the whole understanding of these impurity effect in HTSC have not be achieved in terms of the Fermi liquid theory. By this reason, nontrivial impurity effects in under-doped HTSC's are frequently considered as the evidence of the breakdown of the Fermi liquid state. However, similar impurity effects are observed in other strongly correlated metals such as heavy fermion (HF) systems or organic superconductors, near the magnetic quantum-critical-points (QCP). Therefore, we have to develop previous theories of impurity effect to see whether these experimental results can be explained in terms of the Fermi liquid theory or not.

In HTSC's without impurities, various physical quantities in the normal state deviate from the conventional Fermi liquid behaviors in usual metals, which are called the non-Fermi liquid (NFL) behaviors. Famous examples of the NFL behaviors would be the Curie-Weiss like behavior of $1/T_1T$ and the T -linear resistivity above the pseudo-gap temperature, $T^* \sim 200$ K. One of the most predominant candidates is the Fermi liquid state with

strong antiferromagnetic (AF) fluctuations [1, 2, 3, 4, 5]. In fact, spin fluctuation theories like the SCR theory [2] and the fluctuation-exchange (FLEX) approximation [3, 6, 7, 8, 9, 10] have succeeded in explaining various NFL behaviors in a unified way. Recently, low-energy excitations in connection with HTSC's were studied in ref. [11]. These approximations satisfy the Mermin-Wagner theorem (see Appendix A). Moreover, pseudo-gap phenomena under T^* are well reproduced by the FLEX+ T -matrix approximation, where self-energy correction due to strong superconducting (SC) fluctuations are taken into account [1, 5, 12].

One of the most remarkable NFL behaviors in HTSC's would be the anomalous transport phenomena. For example, the Hall coefficient R_H is proportional to T^{-1} above T^* , and $|R_H| \gg 1/ne$ (n being the electron filling number) at low T [13]. Moreover, the magnetoresistance $\Delta\rho/\rho_0$ is proportional to $R_H^2/\rho_0^2 \propto T^{-4}$, which is called the modified Kohler's rule [14]. They were frequently cited as strong objections against a simple Fermi liquid picture, because analyses based on the relaxation time approximation (RTA) do not work. However, recent theoretical works have revealed that the current vertex corrections (CVC's), which are dropped in the RTA, play important roles in HTSC's. Due to the CVC's, anomalous behaviors of R_H , $\Delta\rho/\rho$, thermoelectric power and Nernst coefficient are naturally explained *in a unified way, based on the Fermi liquid theory* [5, 15, 16, 17, 18].

In the present paper, we study the effect of a single nonmagnetic impurity on a Fermi liquid with strong AF fluctuations. For that purpose, we developed a useful method of calculating the real space structure of the self-

energy and the susceptibility around the strong nonmagnetic impurity, on the basis of an improved FLEX approximation. When the AF fluctuations are strong, we find that both local and staggered spin susceptibilities are enhanced around the impurity. Moreover, the residual resistivity $\Delta\rho$ per impurity, which is determined by the nearly parallel shift of $\rho(T)$, can take a huge value beyond the s-wave unitary scattering limit. In addition, a “Kondo-like” insulating behavior ($d\rho/dT < 0$) emerges in the close vicinity of the AF-QCP. These drastic impurity effects in nearly AF systems come from the fact that the electronic states are modified in a wide range around the impurity, whose radius is approximately AF correlation length, ξ_{AF} . The present study provides a unified understanding for various experimental impurity effect in HTSC’s, *as universal phenomena in nearly AF Fermi liquids*. Any exotic mechanisms (breakdown of the Fermi liquid state) need not to be assumed to explain them.

We find that the simple FLEX approximation does not reproduce reliable electronic states around the impurity. For example, the spin susceptibility $\hat{\chi}^s$ is *reduced* around the impurity. This failure comes from the fact that the feedback effect on the vertex correction for $\hat{\chi}^s$ is neglected in the FLEX approximation. To overcome this difficulty, we propose a modified version of the FLEX approximation, which we call the GV^I -FLEX method.

In the present work, we want to calculate the impurity effect at sufficient low temperatures, say 50K. For this purpose, we have to work on a large real-space cluster with a impurity site, which should be at least 64×64 to obtain the correct bulk electric state at lower temperatures. The FLEX approximation for such a large cluster is, however, almost impossible to perform numerically. Here, we invented the method to calculate the single impurity effect in a large cluster, using the fact that the the range of the modification of electronic states due to the impurity is at least $5 \sim 6$ except for in heavily underdoped systems.

A. Previous Theoretical Studies

Effect of a nonmagnetic impurity embedded in the Hubbard model or in the t - J model had been studied theoretically by various methods. The t - J cluster model (~ 20 sites) with a single nonmagnetic impurity was studied using the exact diagonalization method [19, 20]. They found that the AF correlation is enhanced around the impurity. The same result is realized in two-dimensional Heisenberg models with a vacant site because quantum fluctuations are reduced around the impurity [21, 22]. The same mechanism will account for the enhancement of the AF correlation around an impurity in t - J model. Moreover, in the t - J model, an effective long-range impurity potential is induced due to the many-body effect. The authors discussed that non s-wave scattering given by the effective long-range potential could give rise to a huge residual resistivity per impurity, beyond the s-

wave unitary scattering limit. It is noteworthy that an extended Gutzwiller approximation was applied for the impurity problem in the t - J model [23].

Also, the Hubbard model with a single nonmagnetic impurity was studied using the random phase approximation (RPA) in refs. [24, 25, 26]. By assuming an “extended impurity potential”, they explained that the local susceptibility is enhanced in proportion to χ_Q [$\propto T^{-1}$] of the host, reflecting the lack of translational invariance. Similar analysis based on a phenomenological AF fluctuation model was done [27]. The staggered susceptibilities is also enhanced due to the change of the local DOS (Friedel oscillation) [28]. However, the RPA could not explain the enhancement of local and staggered susceptibilities when the (δ -functional) onsite impurity potential, which corresponds to Zn or Li substitution in HTSC’s, is assumed. Therefore, results given by the RPA are not universal in that they are very sensitive to the strength of extended impurity potential.

In the present work based on the GV^I -FLEX approximation, we show that δ -functional onsite nonmagnetic impurity causes the enhancement of χ^s universally. As a result, onsite impurities cause a huge residual resistivity due to the nonlocal widespread change on the self-energy. We will see that the GV^I -method gives a unified understanding of the impurity problem in HTSC.

B. Experimental Results

Here, we introduce several experimental results in HTSC’s and the related systems, which we focus on in the present work. In later sections, we will discuss the origin of these experimental facts, and show that they are qualitatively well explained in a unified way *as the effect of nonmagnetic impurities or residual disorders*, on the basis of the GV^I -method.

(a) Magnetic properties: In optimally or underdoped HTSC’s, a nonmagnetic impurity replacing a Cu site causes a localized momentum. A Curie like uniform spin susceptibility is induced by dilute doping of Zn in $\text{YBa}_2\text{Cu}_3\text{O}_{7-x}$ (YBCO). The Curie constant C per Zn in under-doped compounds ($x \approx 0.34$) is much larger than that in optimally doped ones ($x \approx 0$) [29]. They also reports an interesting relation $C \propto \Delta\rho$. Curie-like susceptibility was observed in Al-doped $\text{La}_{2-\delta}\text{Sr}_\delta\text{CuO}_4$ (LSCO) [30]. In Zn-doped YBCO compounds, site-selective ^{89}Y NMR measurements revealed that both the local spin susceptibility [31, 32] and the staggered susceptibility [33] are prominently enhanced around the Zn-site, within the radius of the AF correlation length ξ_{AF} . The same result was obtained by the ^7Li Knight shift measurement in Li-doped YBCO compounds [34], and by the ^{63}Cu NMR measurement in Zn-doped YBCO compounds [35]. These NMR studies show that the impurities does not trap holes, contrary to the suggestion by refs. [19, 20]. This fact means that the impurity-induced local moments

result from the change of the magnetic properties of itinerant electrons around the impurity sites.

(b) Resistivity: Fukuzumi et al. observed $\rho(T)$ in Zn-doped YBCO and LSCO for Zn concentration $n_{\text{imp}} = 0.02 \sim 0.04$ [36]. In over-doped systems, the residual resistivity $\Delta\rho(T)$ per impurity, which is determined from nearly parallel shift of $\rho(T)$ by impurities, is consistent with the value for 2D electron gas; $\rho_{\text{imp}}^0 = (4\hbar/e^2)n_{\text{imp}}/n$. However, $\Delta\rho \sim (4\hbar/e^2)n_{\text{imp}}/|1 - n| \gg \rho_{\text{imp}}^0$ in under-doped systems. This fact suggests that the scattering cross section of Zn anomalously increases in under-doped HTSC's, as if an effective radius of impurity potential grows due to many-body effect. In addition, upturn of $\rho(T)$ ($d\rho/dT < 0$) is observed below 50K in under-doped compounds.

Such a prominent enhancement of residual resistivity $\Delta\rho$ is also observed in HF compounds near the AF-QCP, which is realized under a critical pressure P_c [37, 38]. Famous examples are CeCu₅Au ($P_c \approx 3.4$ GPa) [39], CeRhIn₅ ($P_c \approx 2$ GPa) and CeCoIn₅ ($P_c \approx 0$ GPa) [40, 41]. Note that the enhancement of $\Delta\rho$ has nothing to do with the increase of the renormalization factor z ($\ll 1$) by applied pressure, because $\Delta\rho$ is independent of z in the Fermi liquid theory. In addition, the residual resistivity of an organic superconductor κ -(BEDT-TTF)₄Hg_{2.89}Br₈ ($T_c \approx 4$ K), which is close to the AF-QCP at ambient pressure, decreases to be about 10% of the original value by applying the pressure [42]. Such a drastic reduction of $\Delta\rho$ cannot be attributed to the change of the DOS by pressure.

Ando et al. have measured the resistivity in HTSC's under high magnetic field (~ 60 T), which totally suppresses the superconductivity [43, 44]. In LSCO, they found that the insulating behavior emerges under the original T_c at $\mathbf{B} = 0$. This upturn of ρ occurs when $k_Fl \sim 13 \gg 1$ in the ab -plane (l being the mean free path), so it has nothing to do with conventional localization in bad metals. Also, It will be independent of the opening of the pseudo-gap because the pseudo-gap temperature T^* is much higher. Moreover, neither the weak localization or the Kondo effect due to magnetic impurities cannot be the origin of the upturn, because the (negative) magnetoresistance in the insulating region is independent of the field direction, and the insulating behavior persists under very high magnetic field.

Sekitani et al. also found similar insulating behavior ($d\rho/dT < 0$) in under-doped electron-doped systems, $M_{2-\delta}\text{Ce}_\delta\text{CuO}_4$ ($M=\text{Nd, Pr, and La}$), in the normal state under high magnetic field [45]. They discussed that the residual apical oxygens (about 1%), which works as impurity scattering potentials, give rise to the insulating behavior. They expected that the Kondo effect occurs. However, the \mathbf{B} -dependence of $\rho(\mathbf{B}, T)$ does not seem to be consistent with the Kondo effect. The upturn of ρ_c along the c -axis is also observed in optimally doped $\text{Sm}_{2-\delta}\text{Ce}_\delta\text{CuO}_4$ ($\delta \approx 0.14$) in ref. [46]; the upturn is robust against the strong magnetic field (~ 45 T), both

for $\mathbf{B} \parallel \mathbf{a}$ and $\mathbf{B} \parallel \mathbf{c}$. Recently, upturn of ρ in optimally doped PCCO had been observed [47].

(c) Local density of states:

STM measurement [48] revealed that a single nonmagnetic impurity in optimally doped $\text{Bi}_2\text{Sr}_2\text{CaCu}_2\text{O}_{8+\delta}$ causes strong suppression of the superconducting state with radius $\sim 15\text{\AA}$. This "Swiss cheese structure" below T_c had been suggested by the μ -SR measurement [49] as well as the specific heat measurement in Zn doped LSCO [50]. Reference [50] reports that the radius of Swiss cheese hole increases as the carrier doping decreases. The radius is approximately ξ_{AF} , rather than the coherence length. This result suggests that the electronic properties in the Swiss cheese hole is strongly modified even above T_c , because ξ_{AF} is a characteristic length scale in the normal state. Moreover, resent STM/STS measurements have revealed that the local density of states (DOS) in $\text{Bi}_2\text{Sr}_2\text{CaCu}_2\text{O}_{8+x}$ is very inhomogeneous in the atomic scale [51, 52]. The observed ununiformity originates from the weak scattering potentials from out-of-plane dopant atoms [51]. These experimental observations suggest that the DOS and the electronic states in HTSC's are quite sensitive to the disorder potential.

II. FORMALISM

In the present paper, we study a $(N \times N)$ square lattice Hubbard model with an impurity site:

$$H = H_0 + H_{\text{imp}}, \quad (1)$$

$$H_0 = \sum_{\mathbf{k}\sigma} \epsilon_{\mathbf{k}} c_{\mathbf{k}\sigma}^\dagger c_{\mathbf{k}\sigma} + U \sum_i n_{i\uparrow} n_{i\downarrow}, \quad (2)$$

$$H_{\text{imp}} = I(n_{0\uparrow} + n_{0\downarrow}), \quad (3)$$

where H_0 is the Hubbard model for the host system. In H_{imp} , I is the onsite nonmagnetic impurity potential at the origin ($\mathbf{r} = 0$). Because the translational invariance is violated in the case of $I \neq 0$, the self-energy $\Sigma(\mathbf{r}, \mathbf{r}'; \epsilon_n)$ and the Green function $G(\mathbf{r}, \mathbf{r}'; \epsilon_n)$ cannot be functions of $\mathbf{r} - \mathbf{r}'$. In the present paper, we concentrate on the strong impurity potential case (unitary scattering case); $I = \infty$. We will take the $I = \infty$ -limit in the course of the calculation.

We develop the method to study the impurity effect with strong potential on the basis of the FLEX approximation. When $I \neq 0$, Green functions which compose the self-energy for $I = 0$ get insertions of I 's in all possible manners. Then, the self-energy is divided into two terms:

$$\Sigma(\mathbf{r}_i, \mathbf{r}_j; \epsilon_n) = \Sigma^0(\mathbf{r}_i - \mathbf{r}_j; \epsilon_n) + \delta\Sigma(\mathbf{r}_i, \mathbf{r}_j; \epsilon_n), \quad (4)$$

where Σ^0 is the self-energy for $I = 0$, that is, the self-energy for the host system without impurity. $\delta\Sigma$ represents the cross terms between I and U . Here, $\delta\Sigma$ does not contain any terms composed of only I 's. The full Green function for $H_0 + H_{\text{imp}}$ is composed of Σ^0 , $\delta\Sigma$ and I . In

$$\overline{\overline{G^I}} = \overline{\overline{G^0}} + \overline{\overline{G^0}} \times \overline{\overline{G^I}}$$

$$\overline{\overline{G}} = \overline{\overline{G^I}} + \overline{\overline{G^I}} \times \overline{\overline{\delta\Sigma}}$$

$$\delta\Sigma = \Sigma - \Sigma^0$$

FIG. 1: Dyson equations for G^I and G in the presence of I and $\delta\Sigma$.

the case of $I = \infty$, $\delta\Sigma(\mathbf{r}, 0) = -\delta\Sigma(0, \mathbf{r}) = -\Sigma^0(\mathbf{r}, 0)$ because $\Sigma(\mathbf{r}, 0) = \Sigma(0, \mathbf{r}) = 0$. The impurity potential also causes the nonlocal change in the self-energy, that is, $\delta\Sigma(\mathbf{r}_i, \mathbf{r}_j)$ is finite even for $\mathbf{r}_i, \mathbf{r}_j \neq 0$. $\delta\Sigma(\mathbf{r}_i, \mathbf{r}_j)$ will quickly converge to zero as \mathbf{r}_i or \mathbf{r}_j are away from the origin.

The Dyson equation for the real-space Green function in the matrix representation is given by

$$\begin{aligned} \hat{G}(\epsilon_n) &= \hat{G}^{00}(\epsilon_n) + \hat{G}^{00}(\epsilon_n)(\hat{\Sigma}(\epsilon_n) + \hat{I})\hat{G}(\epsilon_n) \\ &= \hat{G}^0(\epsilon_n) + \hat{G}^0(\epsilon_n)(\delta\hat{\Sigma}(\epsilon_n) + \hat{I})\hat{G}(\epsilon_n), \end{aligned} \quad (5)$$

where $(\hat{I})_{i,j} = I\delta_{i,0}\delta_{j,0}$ represents the impurity potential at the origin. $G^{00}(\mathbf{r}_i - \mathbf{r}_j; \epsilon_n) = \frac{1}{N^2} \sum_{\mathbf{k}} (i\epsilon_n + \mu - \epsilon_{\mathbf{k}})^{-1} e^{i\mathbf{k} \cdot (\mathbf{r}_i - \mathbf{r}_j)}$ is the non-interacting Green function, and $\hat{G}^0(\epsilon_n) = ([\hat{G}^{00}(\epsilon_n)]^{-1} - \hat{\Sigma}^0(\epsilon_n))^{-1}$ is the interacting Green function without impurity ($I = 0$).

The Dyson equation is also written as

$$\hat{G}(\epsilon_n) = \hat{G}^I(\epsilon_n) + \hat{G}^I(\epsilon_n)\delta\hat{\Sigma}(\epsilon_n)\hat{G}(\epsilon_n), \quad (6)$$

$$\hat{G}^I(\epsilon_n) = \hat{G}^0(\epsilon_n) + \hat{G}^0(\epsilon_n)\hat{I}\hat{G}^I(\epsilon_n), \quad (7)$$

where \hat{G}^I represents the Green function composed of I and G^0 , that is, $\hat{G}^I = \hat{G}|_{\delta\Sigma=0}$. Equations (6) and (7) are expressed in Fig. 1.

In the present work, we calculate the self-energy for $I \neq 0$ based on the improved FLEX approximation, without taking any averaging with respect to the position of impurity. Hereafter, we propose the three versions of frameworks for calculating the self-energy as follows.

(I) GV^0 -method : First, we introduce the “ GV^0 -FLEX approximation”, where the full Green function G is obtained self-consistently whereas any impurity effects on the effective interaction V^0 are neglected. Here, the self-energy is given by

$$\begin{aligned} \Sigma_{[GV0]}(\mathbf{r}_i, \mathbf{r}_j; \epsilon_n) &= T \sum_l G_{[GV0]}(\mathbf{r}_i, \mathbf{r}_j; \omega_l + \epsilon_n) \\ &\quad \times V^0(\mathbf{r}_i, \mathbf{r}_j; \omega_l), \end{aligned} \quad (8)$$

where $\epsilon_n = (2n + 1)\pi T$ and $\omega_l = 2l \cdot \pi T$, respectively. $G_{[GV0]}$ and $\delta\Sigma_{[GV0]} \equiv \Sigma_{[GV0]} - \Sigma^0$ satisfy the Dyson equation, (6). V^0 and Σ^0 are given by the FLEX approximation for the host system. Hereafter, we call eq. (8)

the GV^0 -method for simplicity, because the self-energy is symbolically written as $G \circ V^0$. Here, V^0 and Σ^0 are given by

$$V^0(\mathbf{r}_i, \mathbf{r}_j; \omega_l) = \frac{1}{N^2} \sum_{\mathbf{q}} V^0(\mathbf{q}, \omega_l) e^{i\mathbf{q} \cdot (\mathbf{r}_i - \mathbf{r}_j)}, \quad (9)$$

$$V^0(\mathbf{q}, \omega_l) = U^2 \left(\frac{3}{2} \chi_{\mathbf{q}}^{0s}(\omega_l) + \frac{1}{2} \chi_{\mathbf{q}}^{0c}(\omega_l) - \Pi_{\mathbf{q}}^0(\omega_l) \right), \quad (10)$$

$$\chi_{\mathbf{q}}^{0s(c)}(\omega_l) = \Pi_{\mathbf{q}}^0(\omega_l) \cdot \{1 - (+)U\Pi_{\mathbf{q}}^0(\omega_l)\}^{-1}, \quad (11)$$

$$\Pi_{\mathbf{q}}^0(\omega_l) = -T \sum_{\mathbf{k}, n} G_{\mathbf{k}+\mathbf{q}}^0(\omega_l + \epsilon_n) G_{\mathbf{k}}^0(\epsilon_n), \quad (12)$$

$$\Sigma_{\mathbf{k}}^0(\epsilon_n) = T \sum_{\mathbf{q}, l} G_{\mathbf{k}+\mathbf{q}}^0(\epsilon_n + \omega_l) V^0(\mathbf{q}, \omega_l), \quad (13)$$

where $G_{\mathbf{k}}^0(\epsilon_n) = (i\epsilon_n + \mu - \epsilon_{\mathbf{k}} - \Sigma_{\mathbf{k}}^0(\epsilon_n))^{-1}$. $\chi_{\mathbf{q}}^{0s}$ and $\chi_{\mathbf{q}}^{0c}$ are spin and charge susceptibilities, respectively, given by the FLEX approximation for the host system.

Using the GV^0 -method, We can calculate the nonlocal change in the self-energy induced around the impurity, $\delta\Sigma$. However, the nonlocal change in the spin susceptibility is not taken into account in the GV^0 -method. To calculate this effect, we introduce other two methods as follows.

(II) GV -method : Next, we explain the “ GV -method”, which is equal to the FLEX approximation in real space. In this method, both the self-energy and the effective interaction are obtained fully self-consistently. The self-energy in the GV -method is given by

$$\begin{aligned} \Sigma_{[GV]}(\mathbf{r}_i, \mathbf{r}_j; \epsilon_n) &= T \sum_l G_{[GV]}(\mathbf{r}_i, \mathbf{r}_j; \omega_l + \epsilon_n), \\ &\quad \times V(\mathbf{r}_i, \mathbf{r}_j; \omega_l) \end{aligned} \quad (14)$$

$$\hat{V}(\omega_l) = U^2 \left(\frac{3}{2} \hat{\chi}^s(\omega_l) + \frac{1}{2} \hat{\chi}^c(\omega_l) - \hat{\Pi}(\omega_l) \right), \quad (15)$$

where $G_{[GV]}$ and $\delta\Sigma_{[GV]} = \Sigma_{[GV]} - \Sigma^0$ satisfy Dyson equation (6). The spin and charge susceptibilities in the GV -method, $\hat{\chi}^s$ and $\hat{\chi}^c$, are given by

$$\hat{\chi}^{s(c)} = \hat{\Pi} \left(1 - (+)U\hat{\Pi} \right)^{-1}, \quad (16)$$

$$\begin{aligned} \Pi(\mathbf{r}_i, \mathbf{r}_j; \omega_l) &= -T \sum_{\epsilon_n} G_{[GV]}(\mathbf{r}_i, \mathbf{r}_j; \epsilon_n + \omega_l) \\ &\quad \times G_{[GV]}(\mathbf{r}_j, \mathbf{r}_i; \epsilon_n). \end{aligned} \quad (17)$$

In the GV -method, the impurity effect on V is fully taken into account in terms of the FLEX approximation. However, we find that the numerical results given by the GV -method are totally inconsistent with experimental facts. This is because the vertex corrections (VC's) for the spin susceptibility, which are dropped in the GV -method, becomes significant in strongly correlated systems. We will discuss this point in §V.

(III) GV^I -method: To overcome the difficulty inherent in the GV -method, we propose the “ GV^I -method”, where the Green function is obtained self-consistently whereas the impurity effect on the effective interaction is calculated in a partially self-consistent way. We will show that the GV^I -method is the most superior among (I)-(III). Here, the self-energy is given by

$$\Sigma_{[GVI]}(\mathbf{r}_i, \mathbf{r}_j; \epsilon_n) = T \sum_l G_{[GVI]}(\mathbf{r}_i, \mathbf{r}_j; \omega_l + \epsilon_n) \times V^I(\mathbf{r}_i, \mathbf{r}_j; \omega_l), \quad (18)$$

$$\hat{V}^I(\omega_l) = U^2 \left(\frac{3}{2} \hat{\chi}^{Is}(\omega_l) + \frac{1}{2} \hat{\chi}^{Ic}(\omega_l) - \hat{\Pi}^I(\omega_l) \right), \quad (19)$$

where $G_{[GVI]}$ and $\delta\Sigma_{[GVI]} = \Sigma_{[GVI]} - \Sigma^0$ satisfy Dyson equation (6). The spin and charge susceptibilities in the GV^I -method, $\hat{\chi}^{Is}$ and $\hat{\chi}^{Ic}$, are given by

$$\hat{\chi}^{Is(c)} = \hat{\Pi} \left(1 - (+)U\hat{\Pi}^I \right)^{-1}, \quad (20)$$

$$\Pi^I(\mathbf{r}_i, \mathbf{r}_j; \omega_l) = -T \sum_{\epsilon_n} G^I(\mathbf{r}_i, \mathbf{r}_j; \epsilon_n + \omega_l) \times G^I(\mathbf{r}_j, \mathbf{r}_i; \epsilon_n). \quad (21)$$

In $\hat{\chi}^{Is}$ and $\hat{\chi}^{Ic}$ in the GV^I -method, the self-energy correction given by the cross terms between I and U [$\delta\Sigma$] is not taken into account, whereas it is taken in the GV -method. Nonetheless, results given by the GV^I -method are completely different from results by the GV -method, and the former results are well consistent with experiments. For example, $\hat{\chi}^{Is}$ given in eq.(20) is strongly enhanced around the impurity, whereas $\hat{\chi}^s$ given in eq.(16) is suppressed by $\delta\Sigma$. In §V, we will show that the latter result is an artifact of the GV -method because the reduction of $\hat{\chi}^s$ due to $\delta\Sigma$ is overestimated. As a result, the GV^I -method is much superior to the GV -method.

Figure 2 expresses the self-energies for GV , GV^I and GV^0 -methods, respectively. These methods are equivalent to the FLEX approximation when $I = 0$. In later sections, we solve the single impurity problem in the presence of the Coulomb interaction on the basis of these three methods.

III. METHOD OF NUMERICAL CALCULATION

In this section, we study the two-dimensional Hubbard model with an impurity potential at the origin. We work on the $(N \times N)$ -square lattice with periodic boundary condition. N should be large (at least 64) enough to achieve the thermodynamic limit at low temperatures. On the other hand, the range of nonlocal change in electronic states due to the impurity is only a few lattice spacings. Taking this fact into account, we calculate $\delta\Sigma_{\alpha,\beta}$ (α and β being the lattice points in real space) by the

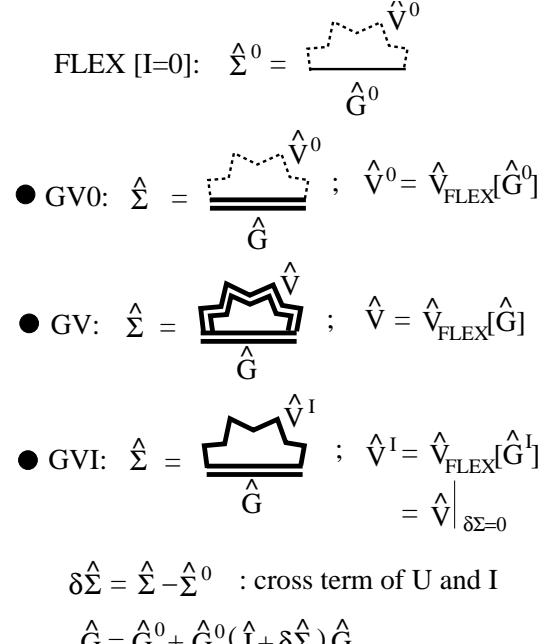


FIG. 2: Self-energy for the Hubbard model with a nonmagnetic impurity, given by the GV , GV^I and GV^0 -method.

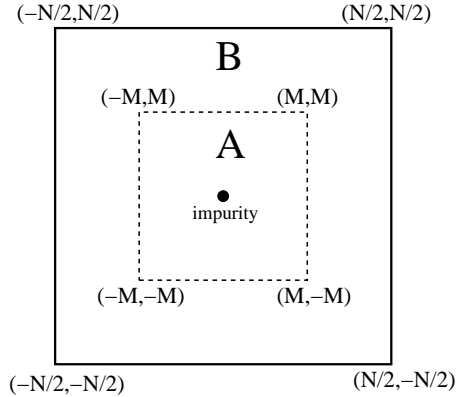


FIG. 3: Schematic expression for region A and B.

(improved) FLEX approximation only for $|\alpha|, |\beta| \leq M$ ($M \ll N$), and we put $\delta\Sigma_{\alpha,\beta} = 0$ for $|\alpha| > M$ or $|\beta| > M$. Here we put $M = 6 \sim 8$, which is enough to obtain a reliable numerical result. Here, we explain the method how to reduce the working area to a $((2M + 1) \times (2M + 1))$ -square lattice in solving the single impurity problem in the $(N \times N)$ -square lattice. This technique helps us to avoid considerable numerical difficulty. Hereafter, we use i, j, \dots (α, β, \dots) to represent the lattice points in the region A+B (region A) in Fig.3.

According to eq.(7), $G_{i,j}^I$ is given by

$$G_{0,j}^I = G_{j,0}^I = \frac{G_{0,j}^0}{1 - I G_{0,0}^0}, \quad (22)$$

$$G_{i,j}^I = G_{i,j}^0 + I \frac{G_{i,0}^0 G_{0,j}^0}{1 - I G_{0,0}^0} \quad \text{for } i, j \neq 0, \quad (23)$$

where $G_{i,j}^0(\epsilon_n) = G^0(\mathbf{r}_i, \mathbf{r}_j; \epsilon_n) = G^0(\mathbf{r}_i - \mathbf{r}_j; \epsilon_n) = \frac{1}{N^2} \sum_{\mathbf{k}} G_{\mathbf{k}}^0(\epsilon_n) \exp(i\mathbf{k} \cdot (\mathbf{r}_i - \mathbf{r}_j))$; $G_{\mathbf{k}}^0(\epsilon_n)$ is the Green function given by the FLEX approximation without impurity potential. Therefore, $G_{i,j}^I$ in the limit of $I = \infty$ is

$$G_{0,j}^I = G_{j,0}^I = 0, \quad (24)$$

$$G_{i,j}^I = G_{i,j}^0 - \frac{G_{i,0}^0 G_{0,j}^0}{G_{0,0}^0} \quad \text{for } i, j \neq 0. \quad (25)$$

According to eq.(6), the Dyson equation for the full Green function $G_{\alpha,\beta}$ inside of region A is given by

$$G_{\alpha,\beta} = G_{\alpha,\beta}^I + \sum_{\beta'}^A A_{\alpha,\beta'} G_{\beta',\beta}, \quad (26)$$

$$A_{\alpha,\beta} = \sum_{\beta'}^A G_{\alpha,\beta'}^I \delta \Sigma_{\beta',\beta}. \quad (27)$$

Note that $\delta \Sigma_{\alpha,\beta}$ is finite only when both α and β are inside of region A in the present approximation. By solving eq.(26), we obtain

$$\hat{G}(\epsilon_n) = \left(\hat{1} - \hat{A}(\epsilon_n) \right)^{-1} \hat{G}^I(\epsilon_n), \quad (28)$$

which is a $((2M+1)^2 \times (2M+1)^2)$ -matrix equation. In the limit of $I = \infty$, $G_{\alpha,\beta}$ is given by

$$G_{\alpha,\beta} = \sum_{\delta \neq 0}^A \left(\hat{1} - \hat{A} \right)_{\alpha\delta}^{-1} \left(G_{\delta,\beta}^0 - \frac{G_{\delta,0}^0 G_{0,\beta}^0}{G_{0,0}^0} \right) \quad (29)$$

Note that $G_{\alpha,0} = G_{0,\beta} = 0$. $A_{\alpha,\beta}$ in eq.(29) is given by

$$A_{\alpha,\beta} = D_{\alpha\beta}^0 - \frac{G_{\alpha,0}^0}{G_{0,0}^0} D_{0,\beta}^0, \quad (30)$$

$$D_{\alpha,\beta}^0 = \sum_{\beta'}^A G_{\alpha,\beta'}^0 \delta \Sigma_{\beta',\beta}. \quad (31)$$

Next, we study the spin and charge susceptibilities in the presence of an impurity. In the FLEX approximation, the equation for the magnetic susceptibility in real space is

$$\chi_{i,j}^s = \Pi_{i,j} + U \sum_l^{A+B} \Pi_{i,l} \chi_{l,j}^s, \quad (32)$$

where i , j and l represent the lattice points in region A+B. $\Pi_{i,j}$ is the irreducible susceptibility defined in eq.(17) in the GV-method or in eq.(21) in the GV^I -method. This equation is not easy to solve because of its huge matrix size; $(N^2 \times N^2)$. To solve this difficulty, we reduce the above equation to $((2M+1)^2 \times (2M+1)^2)$ -matrix equation (inside of region A), approximating that

$\Pi_{i,j} = \Pi_{i-j}^0$ when i and/or j are in region B. Here, Π_{i-j}^0 is the irreducible susceptibility for the host system: $\Pi_{i-j}^0(\omega_l) = -T \sum_{\epsilon_n} G_{i-j}^0(\epsilon_n + \omega_l) G_{j-i}^0(\epsilon_n)$.

Here, $\chi_{\alpha,\beta}^s$ inside region A is rewritten as

$$\begin{aligned} \chi_{\alpha,\beta}^s &= \Pi_{\alpha,\beta} + U \sum_{\gamma \neq 0}^A \Pi_{\alpha,\gamma} \chi_{\gamma,\beta}^s \\ &\quad + \delta \chi_{\alpha,\beta}^s + U \sum_{\gamma \neq 0}^A \delta \chi_{\alpha,\gamma}^s \chi_{\gamma,\beta}^s, \end{aligned} \quad (33)$$

$$\begin{aligned} \delta \chi_{\alpha,\beta}^s &= U \sum_l^B \Pi_{\alpha,l}^0 \Pi_{l,\beta}^0 \\ &\quad + U^2 \sum_{l,m} \Pi_{\alpha,l}^0 \Pi_{l,m}^0 \Pi_{m,\beta}^0 + \dots \end{aligned} \quad (34)$$

The infinite series of summation in eq.(34) can be taken by using the following fact: In the case of $I = 0$, eq.(33) gives $\chi_{\alpha-\beta}^{0s} \equiv \frac{1}{N^2} \sum_{\mathbf{k}} \Pi_{\mathbf{k}}^0 (1 - U \Pi_{\mathbf{k}}^0)^{-1} \exp(i\mathbf{k} \cdot (\mathbf{r}_\alpha - \mathbf{r}_\beta))$. As a result, we obtain that

$$\begin{aligned} \chi_{\alpha,\beta}^{0s} &= \Pi_{\alpha,\beta}^0 + U \sum_{\gamma}^A \Pi_{\alpha,\gamma}^0 \chi_{\gamma,\beta}^{0s} \\ &\quad + \delta \chi_{\alpha,\beta}^s + U \sum_{\gamma}^A \delta \chi_{\alpha,\gamma}^s \chi_{\gamma,\beta}^{0s}, \end{aligned} \quad (35)$$

$$(36)$$

where the summation of γ contains the origin. By solving this $((2M+1)^2 \times (2M+1)^2)$ -matrix equation, $\delta \chi^s$ is obtained as

$$\hat{\delta \chi}^s = \left(\hat{\chi}^{0s} - \hat{\Pi}^0 - U \hat{\Pi}^0 \hat{\chi}^{0s} \right) (1 + U \hat{\chi}^{0s})^{-1}. \quad (37)$$

Using eq.(37), the solution of eq.(33) is given by

$$\hat{\chi}^s = \left(1 - U \hat{\Pi} - U \hat{\delta \chi}^{s*} \right)^{-1} \left(\hat{\Pi} + \hat{\delta \chi}^{s*} \right), \quad (38)$$

$$\delta \chi_{\alpha,\beta}^{s*} \equiv \delta \chi_{\alpha,\beta}^s (1 - \delta_{\alpha\beta,0}), \quad (39)$$

where the factor $1 - \delta_{\alpha\beta,0}$ in eq. (39) represents the elimination of $\gamma = 0$ in the summation in eq. (33). Numerical calculation of eq.(38) is easy because its matrix size $((2M+1)^2 \times (2M+1)^2)$ is not large for $M = 6 \sim 8$. In the numerical study, we have to check that all the eigenvalues of $1 - U \hat{\Pi} - U \hat{\delta \chi}^{s*}$ in eq.(38) are positive, because a single impurity in a paramagnetic bulk system could not induce a static magnetic order.

In the same way, we derive the charge susceptibility, which is given by the following $(N^2 \times N^2)$ -matrix equation:

$$\chi_{i,j}^c = \Pi_{i,j} - U \sum_l^{A+B} \Pi_{i,l} \chi_{l,j}^c. \quad (40)$$

Taking the same procedure as used in deriving eq.(38), $\chi_{\alpha,\beta}^c$ in the region A is given by the following $((2M+1)^2 \times (2M+1)^2)$ -matrix:

$$\hat{\chi}^c = \left(1 + U\hat{\Pi} + U\hat{\delta\chi}^{c*} \right)^{-1} \left(\hat{\Pi} + \hat{\delta\chi}^{c*} \right). \quad (41)$$

Here, $\hat{\delta\chi}_{\alpha,\beta}^{c*}$ is given by

$$\delta\chi_{\alpha,\beta}^{c*} \equiv \delta\chi_{\alpha,\beta}^c (1 - \delta_{\alpha\beta,0}), \quad (42)$$

$$\hat{\delta\chi}^c = \left(\hat{\chi}^{0c} - \hat{\Pi}^0 + U\hat{\Pi}^0\hat{\chi}^{0c} \right) (1 - U\hat{\chi}^{0c})^{-1}, \quad (43)$$

where $\chi_{i-j}^{0c} = \frac{1}{N^2} \sum_{\mathbf{k}} \Pi_{\mathbf{k}}^0 (1 + U\Pi_{\mathbf{k}}^0)^{-1} \exp(i\mathbf{k} \cdot (\mathbf{r}_i - \mathbf{r}_j))$ is the charge susceptibility for the host system.

Finally, the spin and charge susceptibilities in the GV^I -method, $\hat{\chi}^{Is}$ and $\hat{\chi}^{Ic}$, are obtained as follows:

$$\hat{\chi}^{Is} = \left(1 - U\hat{\Pi}^I - U\hat{\delta\chi}^{s*} \right)^{-1} \left(\hat{\Pi}^I + \hat{\delta\chi}^{s*} \right), \quad (44)$$

$$\hat{\chi}^{Ic} = \left(1 + U\hat{\Pi}^I + U\hat{\delta\chi}^{c*} \right)^{-1} \left(\hat{\Pi}^I + \hat{\delta\chi}^{c*} \right), \quad (45)$$

where $\hat{\Pi}^I$ is given in eq.(21). Note that we have to check that all the eigenvalues of $1 - U\hat{\Pi}^I - U\hat{\delta\chi}^{s*}$ in eq.(44) are positive in the numerical study.

IV. NUMERICAL RESULTS FOR LOCAL DOS AND SPIN SUSCEPTIBILITIES

In this section, we show several numerical results given by GV^0 , GV^I and GV methods. In each methods, the self-energy is obtained self-consistently. We find that GV^I -method gives the most reliable results, irrespective that the fully self-consistent condition for the quasiparticle interaction is not imposed. In the GV -method, on the other hand, the reduction of χ^s due to $\delta\Sigma$ [i.e., the non-local change in the self-energy given by the cross terms between I and U] is overestimated. In §V, we will show that the reduction of V due to $\delta\Sigma$ is almost recovered if one takes account of the VC due to the excess spin fluctuations induced by the impurity. By this reason, the GV^I -method is the most reliable formalism. In the present section, we mainly focus on the numerical results given by the GV^I -method.

In the present numerical study, the dispersion of the conduction electron is given by

$$\epsilon_{\mathbf{k}} = 2t(\cos(k_x) + \cos(k_y)) + 4t' \cos(k_x) \cos(k_y) + 2t''(\cos(2k_x) + \cos(2k_y)), \quad (46)$$

where t , t' , and t'' are the nearest, the next nearest, and the third nearest neighbor hopping integrals, respectively. In the present study, we use the following set of parameters: (I) YBCO (hole-doped): $t_0 = -1$, $t_1 = 1/6$, $t_2 = -1/5$, $U = 6 \sim 8$. (II) NCCO (electron-doped): $t_0 = -1$, $t_1 = 1/6$, $t_2 = -1/5$, $U = 5.5$. (III) LSCO (hole-doped): $t_0 = -1$, $t_1 = 1/10$, $t_2 = -1/10$,

$U = 4 \sim 5$. These hopping parameters are equal to those used in ref.[15]. They were determined qualitatively by fitting to the Fermi surface (FS) given by ARPES measurements or the LDA band calculations. The shape of the FS's for (I)-(III), all of which are hole-like, are shown in ref. [15]. Because $t_0 \sim 4000$ K in real systems, $T = 0.01$ corresponds to ~ 40 K. In the present numerical study, 64×64 \mathbf{k} -meshes and 1024 Matsubara frequencies are used.

The value of U used in the present study is rather smaller than the bandwith (W_{band}), irrespective that the real coulomb interaction is larger than W_{band} . This will be justified by considering that U used here is the *effective* Coulomb interaction U_{eff} between quasiparticles with low energies. In fact, $U_{\text{eff}} \sim W_{\text{band}}$ according to the Kanamori theory based on the two-particle approximation [53].

In Ref.[15], the shape of the Fermi surface, the temperature and the momentum dependences of the spin susceptibility [$\chi_{\mathbf{q}}^s(0)$] and the quasiparticle damping rate [$\text{Im}\Sigma_{\mathbf{q}}(-i\delta)$] given by the FLEX approximation are explained in detail. The obtained results are well consistent with experiments. For example, the \mathbf{q} -dependence of $\chi_{\mathbf{q}}^s(0)$ shows that $\xi_{\text{AF}} = 2 \sim 3a$ in YBCO ($n=0.85$) at $T = 0.02$, which is consistent with neutron measurements.

A. Local Density of States

Figure 4 represents the density of states (DOS) for a hole-doped system (LSCO, $n = 0.9$) at $T = 0.02$, at the nearest-neighbor site ($\mathbf{r} = (1,0)$) and the next-nearest-neighbor site ($\mathbf{r} = (1,1)$) of the impurity, respectively. Here, “host” represents the DOS without the impurity given by the FLEX approximation, $N_{\text{host}}(\omega) \equiv \frac{1}{\pi N^2} \sum_{\mathbf{k}} \text{Im}G_{\mathbf{k}}^0(\omega - i\delta)$. On the other hand, $N_l^I(\omega) \equiv \frac{1}{\pi} \text{Im}G_{l,l}^I(\omega - i\delta)$ at site l , where \hat{G}^I is given in eq. (25). In $N_l^I(\omega)$, effect of $\delta\Sigma$ induced around the impurity is dropped. At $(1,0)$ [at $(1,1)$], $N_l^I(\omega)$ is larger [smaller] than $N_{\text{host}}(\omega)$, which is recognized as the Friedel oscillation [28]. This result is changed only slightly by GV^0 or GV methods, which are not shown in 4. However, the DOS given by the GV^I -method is much smaller than $N_l^I(\omega)$ in under-doped systems, because $\text{Im}\delta\Sigma$ takes a large value around the impurity. The Green function is given by

$$\hat{G}_{[\text{GVI}]} = \left([\hat{G}^I]^{-1} - \hat{\delta\Sigma}_{[\text{GVI}]} \right)^{-1}, \quad (47)$$

which are easily obtained by eq.(29) in the present numerical study. As shown in Fig. 4, the local DOS given by the GV^I -method is strongly suppressed, especially at $(1,0)$. This suppression becomes more prominent for $U = 5$. The reason for this suppression is the extremely short quasiparticle lifetime, which is caused by the huge local spin susceptibility $\hat{\chi}^{Is}$ around the impurity. We will

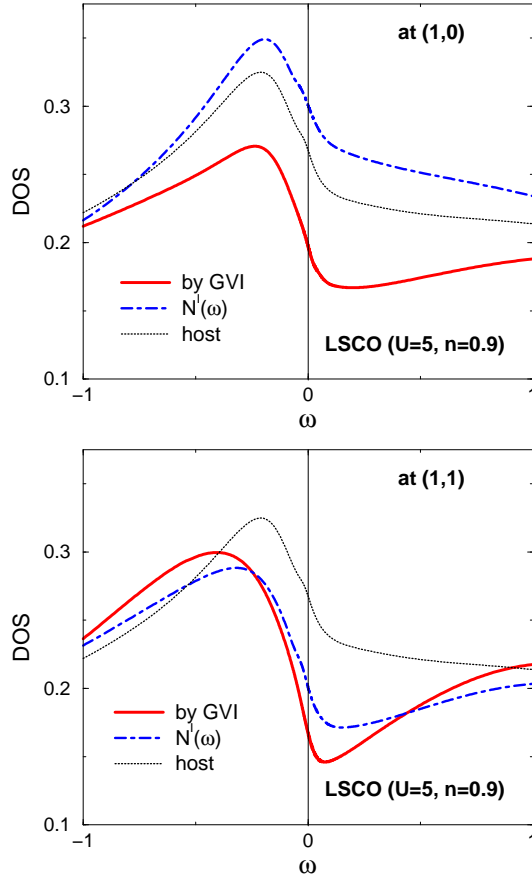


FIG. 4: (Color online) Obtained local DOS for LSCO ($n = 0.9$, $U = 5$) at $T = 0.02$ (~ 80 K). (i)host: DOS given by the FLEX approximation without impurity. (ii) $N_l^I(\omega) = -\frac{1}{N^2} \sum_{\mathbf{k}} \text{Im}G^I(\omega)$ where G^I is given in eq.(25). (iii) local DOS given by the GV^I -method; $-\frac{1}{N^2} \sum_{\mathbf{k}} \text{Im}G_{[\text{GVI}]}(\omega)$

discuss the impurity effect on the spin susceptibility in the next subsection.

Figure 5 shows the reduction of the local DOS at the Fermi level obtained by the GV^I -method, both for hole-doped and electron-doped systems at $T = 0.02$. We see that the DOS is prominently suppressed in a wide region around the impurity, especially along the diagonal axis. The suppression of the DOS is also recognized along x , y -axis, which is caused by the enhanced quasiparticle damping, $\text{Im}\delta\Sigma(-i\delta)$, given by the GV^I -method. The strong suppression of the DOS around the impurity site is consistent with the ‘‘Swiss cheese structure’’ observed in the STM measurement [48]. For LSCO, the radius of the Swiss cheese hole in Fig. 5 is about $3a$ (a being the lattice spacing). It increases further for $U = 5$, approximately in proportion to the AF correlation length $\xi_{\text{AF}}(\propto \sqrt{T})$. Because quasiparticle lifetime is extremely short in the Swiss cheese hole, small number of impurities will induce the huge residual resistivity and the prominent reduction of T_c in under-doped systems. In §VIB,

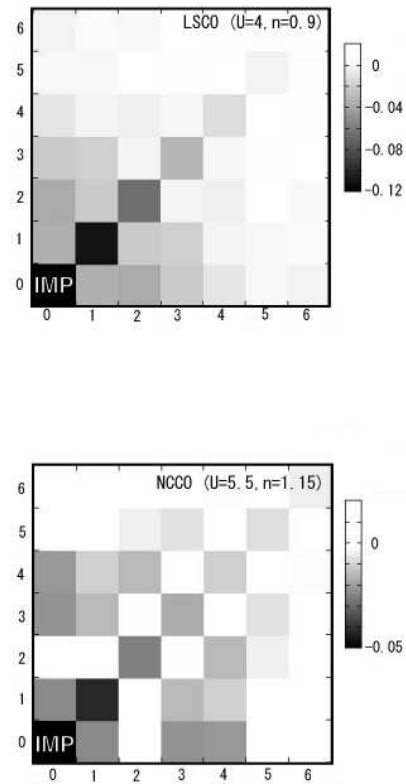


FIG. 5: The reduction of the local DOS at the Fermi level around the impurity given by the GV^I -method, both for LSCO ($n = 0.9$, $U = 4$) and for NCCO ($n = 1.15$, $U = 5.5$) at $T = 0.02$, respectively. In the host, $N_{\text{host}}(0) = 0.322$ for LSCO and $N_{\text{host}}(0) = 0.217$ for NCCO, respectively.

we will calculate the residual resistivity and confirm this expectation.

B. Static Spin Susceptibilities

Figure 6 shows the obtained local spin susceptibility $\chi^s(\mathbf{r}, \mathbf{r})$ along $(1, 0)$ and $(1, 1)$ directions at $T = 0.02$. We see that $\chi^s(\mathbf{r}, \mathbf{r})$ is significantly enhanced around the impurity as U increases, or as n approaches unity. The radius of area where χ^s is enhanced is about $3 \sim 4a$, which would corresponds to the Swiss cheese hole in the DOS. This result is consistent with the impurity effect in under-doped HTSC’s observed by NMR measurements. On the other hand, an opposite result is given by the GV -method, which is not reliable as discussed above. Note that we have checked that all the eigenvalues of $1 - U\hat{\Pi} - U\hat{\delta}\chi^{s*}$ in eq.(38) are positive in the present numerical study.

Figure 7 represents the uniform susceptibility

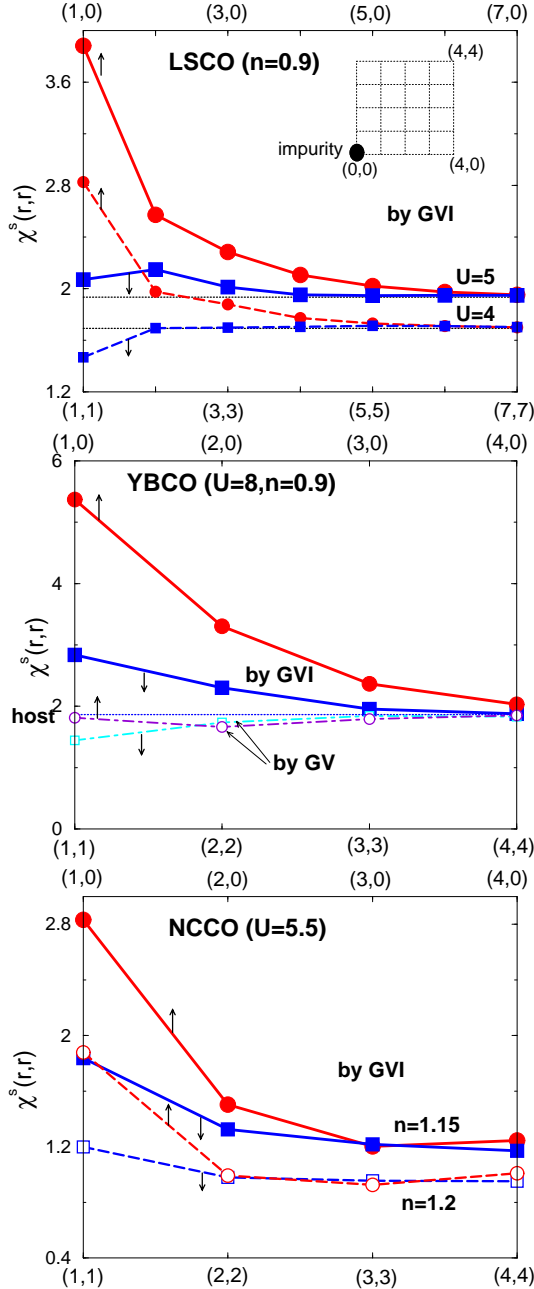


FIG. 6: (Color online) Obtained local spin susceptibility $\chi_s^s(\mathbf{r}, \mathbf{r})$ for LSCO, YBCO and NCCO at $T = 0.02$. Around the impurity site, $\chi_s^s(\mathbf{r}, \mathbf{r})$ is strongly enhanced in the GV^I -method, whereas it slightly decreases in the GV -method. The former result is consistent with experiments.

$\chi_{\text{uniform}}^s = N^{-2} \sum_{i,j} \chi_{i,j}^{Is}(0)$ for LSCO ($n = 0.9$, $U = 5$) given by the GV^I -method. n_{imp} is the concentration of the nonmagnetic impurity. Here, each impurity is assumed to be independent. We see that the uniform susceptibility without impurity decreases slightly at lower temperatures, which corresponds to the “weak pseudo-gap behavior” in HTSC’s above the strong

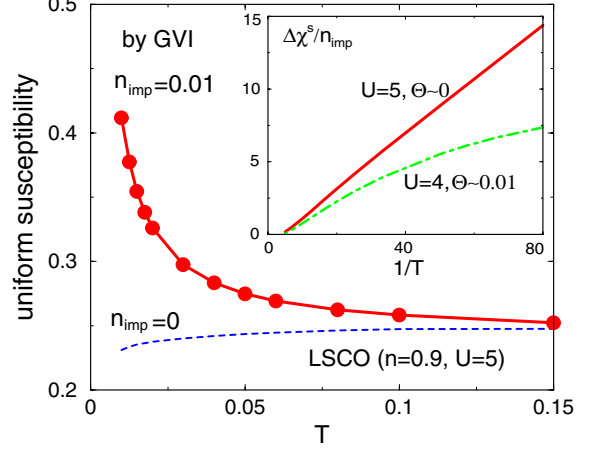


FIG. 7: (Color online) T dependence of the uniform spin susceptibility given by the GV^I -method in the presence or the absence of impurities. Θ represents the Weiss temperature.

pseudo-gap temperatures, $T^* \sim 200$ K. Surprisingly, Fig. 7 shows that a nonmagnetic impurity induces an approximate Curie-Weiss like uniform susceptibility $\Delta\chi \approx n_{\text{imp}} \cdot \mu_{\text{eff}}^2 / 3(T + \Theta)$. For $U = 5$, $\mu_{\text{eff}} = 0.74\mu_B$ and $\Theta = 0$, which means that 42% of a magnetic moment of spin- $\frac{1}{2}$ ($\mu_{\text{eff}} = 1.73\mu_B$) is induced by a single nonmagnetic impurity. A similar behavior is obtained for YBCO in the present study. The obtained induced moment is slightly smaller than the experimental value $\mu_{\text{eff}} \sim 1\mu_B$ in $\text{YBa}_2\text{Cu}_3\text{O}_{6.66}$ ($T_c \approx 60$ K) [29]. In the present calculation, a simple relation $\Delta\chi \propto \chi_Q^0$ predicted by previous theoretical studies [24, 25, 26, 27] approximately holds. The obtained μ_{eff} is the present study is much larger and consistent with experiments.

Figure 8 shows the nonlocal spin susceptibility around the impurity given by the GV^I -method, $\chi^s(\mathbf{r}, \mathbf{r}')$. This result means that staggered susceptibility given by the GV^I -method is strongly enhanced around the impurity. On the other hand, it is slightly suppressed in the GV -method. We consider that the former result is correct whereas the latter result is an artifact of the GV -method because of the lack of the vertex corrections. (see §V.)

Here, we discuss the origin of the enhancement of χ^{Is} : Reflecting the large $N_l^I(\omega)$ at $l = (1,0)$, the absolute value of $\Pi_{i,j}^I(0)$ in the GV^I -method is strongly enhanced especially for $i = (1,0)$ and (a) $j = (1,0)$, (b) $j = (1,1)$, and (c) $j = (2,1)$. In the case of LSCO ($U = 4$, $n = 0.9$) at $T = 0.02$, $\Pi_{i,j}^I(0)$ [$\Pi_{i-j}^0(0)$] becomes 0.172 [0.160] for (a), -0.160 [-0.100] for (b), and 0.104 [0.0784] for (c). This fact will give the enhancement of $\hat{\chi}^{Is} = \hat{\Pi}^I(1 - U\hat{\Pi}^I)^{-1}$ around the impurity site since eigenvalues of $(1 - U\hat{\Pi}^I)$ become smaller. In contrast, an “on-site” nonmagnetic impurity does not give the enhancement of spin susceptibility in the RPA [24, 25, 26]. The reason would be that the strong reduction of $\hat{\Pi}^0$ due to thermal and quantum fluctuations are well de-

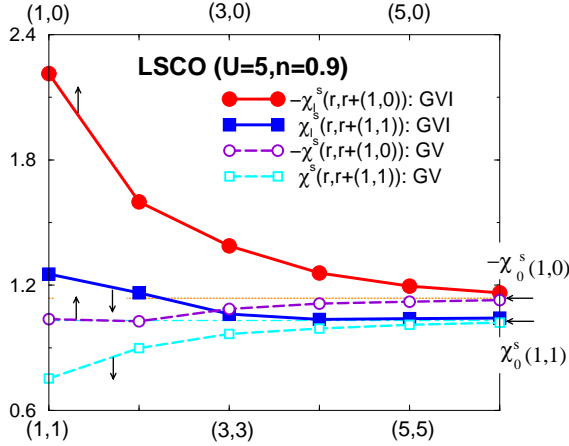


FIG. 8: (Color online) Nonlocal spin susceptibilities $\chi^s(\mathbf{r}, \mathbf{r}')$ for LSCO at $T = 0.02$ given by the GV and GV^I -methods. Around the impurity site, the staggered susceptibility is enhanced in the GV^I -method, whereas it decreases in the GV -method. The former result is consistent with experiments.

scribed in the FLEX approximation. Then, the reduction of fluctuations due to an impurity would give rise to the enhancement of susceptibilities.

In summary, we find that both local and staggered spin susceptibilities are increased around the impurity site, within the radius of about $3a$ ($\sim \xi_{AF}$) at $T = 0.02$. Similar results were obtained for both the hole-doped systems (YBCO and LSCO) and the electron-doped ones (NCCO), rather insensitive to model parameters. Moreover, similar impurity effects were obtained in the t - J model, by exact diagonalization studies [19, 20]. As a result, the obtained impurity effects in this section will be universal in systems close to the AF-QCP.

V. FEEDBACK EFFECT AND VERTEX CORRECTIONS

In previous sections, we show that the local spin susceptibility given by the GV^I -method, χ^{Is} , is prominently enhanced around the impurity. However, χ^{Is} could be modified if we go beyond the GV^I -method be-

cause the induced susceptibility around the impurity, $\Delta\chi \equiv \chi^{Is} - \chi^{0s}$, changes the susceptibility itself, in the form of the self-energy correction ($\delta\Sigma$) and the vertex correction (VC). We call this self-interaction effect “the feedback effect”. In the feedback effect, the susceptibility is enhanced by the VC whereas it is reduced by $\delta\Sigma$. In the GV -method, where only the latter effect is taken into account, the local susceptibility becomes smaller than the host’s value. This inconsistent result suggests the importance of the VC’s. In the present section, we study the VC’s for the spin susceptibility, and show that the VC’s almost cancel the self-energy correction. We find that the total feedback effect is very small in the GV -method with

$$\begin{aligned}
 \text{GVI: } \Pi_I^{I,\sigma\sigma} &= \text{Diagram of a loop with } G^I \text{ and } \sigma \text{ on the lines.} \\
 \text{GV: } \Pi^{\sigma\sigma} &= \text{Diagram of a loop with } G \text{ and } \sigma \text{ on the lines.} \quad \approx \quad \text{Diagram of a loop with } \Delta V \text{ and } G^I \text{ on the lines.} + \text{Diagram of a loop with } \sigma \text{ and } \Delta V \text{ on the lines.} \\
 &\quad \text{---} = \text{Diagram of a loop with } \Delta V \text{ and } V^I \text{ on the lines.} - \text{Diagram of a loop with } \Delta V \text{ and } V^0 \text{ on the lines.} \\
 \Delta\Pi_{MT}^{\sigma\sigma} &= \text{Diagram of a loop with } \Delta V \text{ and } G^I \text{ on the lines.} \\
 \Delta\Pi_{AL}^{\sigma\sigma} &= \text{Diagram of a loop with } V^I \text{ and } \sigma \text{ on the lines.} - \text{Diagram of a loop with } V^0 \text{ and } \sigma \text{ on the lines.} \\
 \Pi_{GV+VC}^{\sigma\sigma} &= \Pi^{I,\sigma\sigma} + \Delta\Pi_{MT}^{\sigma\sigma} + \Delta\Pi_{AL}^{\sigma\sigma}.
 \end{aligned}$$

FIG. 9: Irreducible susceptibilities given by the GV^I , GV and $GV+VC$ methods, respectively.

VC’s ($GV+VC$ -method): The obtained spin susceptibility is similar to that by the GV^I -method. Therefore, we conclude that the GV^I -method is superior to the GV -method.

The irreducible susceptibility given by GV^I -method ($\Pi^{I,\sigma\sigma}$) and GV -method ($\Pi^{\sigma\sigma}$) are expressed in eqs.(17) and (21), respectively. Hereafter, we discuss the feedback effect for the irreducible susceptibility perturbatively with respect to $\Delta\hat{V} = \hat{V}^I - \hat{V}^0$. In this respect, $\Pi^{\sigma\sigma}$ can be expanded with respect to $\Delta\hat{V}$ as

$$\Pi_{i,j}^{\sigma\sigma}(0) \approx \Pi_{i,j}^{I,\sigma\sigma} - 2T \sum_{i',j',\epsilon_m,\epsilon_n} G_{j',j}^I(\epsilon_n) G_{j,i}^I(\epsilon_n) G_{i,i'}^I(\epsilon_n) \cdot \Delta V_{i',j'}(\epsilon_n - \epsilon_m) G_{i',j'}^I(\epsilon_m), \quad (48)$$

up to the lowest order, which is expressed in Fig. 9. We have checked numerically that eq. (48) is satisfied well.

Next, we study the VC for irreducible susceptibility up to the second-order with respect to $\Delta\hat{V}$. The lowest order term, which we call the Maki-Thompson (MT) term customarily, is given by

$$\Delta\Pi_{MT}^{\uparrow\uparrow}(i,j) = -\frac{U^2 T^2}{2} \sum_{i',j';\epsilon_m,\epsilon_n} F(i,j,i',j';\epsilon_m,\epsilon_n) (\Delta\chi_{i',j'}^s(\epsilon_m - \epsilon_n) + \Delta\chi_{i',j'}^c(\epsilon_m - \epsilon_n)), \quad (49)$$

$$\Delta\Pi_{\text{MT}}^{\uparrow\downarrow}(i,j) = -\frac{U^2 T^2}{2} \sum_{i',j';\epsilon_m,\epsilon_n} F(i,j,i',j';\epsilon_m,\epsilon_n) \Delta\chi_{i',j'}^s(\epsilon_m - \epsilon_n), \quad (50)$$

$$\Delta\chi_{i,j}^{s,c} = \chi_{i,j}^{Is,c} - \chi_{i,j}^{0s,c}, \quad (51)$$

$$F(i,j,i',j';\epsilon_m,\epsilon_n) = G_{j',i}^I(\epsilon_m) G_{i',i}^I(\epsilon_m) G_{i',j}^I(\epsilon_n) G_{j',j'}^I(\epsilon_n), \quad (52)$$

which is shown in Fig. 9. We also discuss the second-order term given as

$$\begin{aligned} \Delta\Pi_{\text{AL}}^{\sigma\sigma'}(i,j) &= T \sum_{i_1,i_2,j_1,j_2;\omega_l} F'(i,i_1,i_2;\omega_l) (F'(j,j_1,j_2;\omega_l) + F'(j,j_1,j_2;-\omega_l)) \\ &\quad \times (X_{\sigma\sigma'}^I(i_1,i_2,j_1,j_2;\omega_l) - X_{\sigma\sigma'}^0(i_1,i_2,j_1,j_2;\omega_l)), \end{aligned} \quad (53)$$

$$F'(i,i_1,i_2;\omega_l) = T \sum_{\epsilon_n} G_{i_2,i}^I(\epsilon_n) G_{i_1,i}^I(\epsilon_n) G_{i_1,i_2}^I(\epsilon_n + \omega_l), \quad (54)$$

$$\begin{aligned} X_{\uparrow\uparrow}^{\xi}(i_1,i_2,j_1,j_2;\omega_l) &= \frac{5U^4}{4} \chi_{i_1,j_1}^{\xi s} \chi_{i_2,j_2}^{\xi s} + \frac{U^3}{4} \chi_{i_1,j_1}^{\xi s} (U \chi_{i_2,j_2}^{\xi c} + 4\delta_{i_2,j_2}) + \frac{U^3}{4} \chi_{i_2,j_2}^{\xi s} (U \chi_{i_1,j_1}^{\xi c} + 4\delta_{i_1,j_1}) \\ &\quad + \frac{U^4}{4} \chi_{i_1,j_1}^{\xi c} \chi_{i_2,j_2}^{\xi c}, \end{aligned} \quad (55)$$

$$\begin{aligned} X_{\uparrow\downarrow}^{\xi}(i_1,i_2,j_1,j_2;\omega_l) &= \frac{U^4}{4} (\chi_{i_1,j_1}^{\xi s} - \chi_{i_1,j_1}^{\xi c}) (\chi_{i_2,j_2}^{\xi s} - \chi_{i_2,j_2}^{\xi c}) + \frac{U^3}{2} \delta_{i_1,j_1} (\chi_{i_2,j_2}^{\xi s} - \chi_{i_2,j_2}^{\xi c}) \\ &\quad + \frac{U^3}{2} \delta_{i_2,j_2} (\chi_{i_1,j_1}^{\xi s} - \chi_{i_1,j_1}^{\xi c}), \end{aligned} \quad (56)$$

where $\xi = 0$ or I . We call eq.(53) the Aslamazov-Larkin term.

In the FLEX approximation, the irreducible VC's given by the Ward identity, $\Gamma^{\text{irr}} = \delta\Sigma/\delta G$, are composed of the MT-term and the AL-term [6].

As a result, the irreducible susceptibility given by the "GV-method with VC's up to the second-order with respect to $\Delta\chi^{s,c}$ " (GV+VC method) is given by

$$\begin{aligned} \Pi^{\sigma\sigma'}(i,j) &= \Pi(i,j) \delta_{\sigma,\sigma'} \\ &\quad + \Delta\Pi_{\text{MT}}^{\sigma\sigma'}(i,j) + \Delta\Pi_{\text{AL}}^{\sigma\sigma'}(i,j). \end{aligned} \quad (57)$$

The spin susceptibility in the GV+VC method is obtained as

$$\hat{\chi}_{\text{GV+VC}}^s = \hat{\chi}_{\uparrow\uparrow} + \hat{\chi}_{\uparrow\downarrow}, \quad (58)$$

$$\hat{\chi}_{\uparrow\uparrow} = \hat{\Pi}_{\uparrow\uparrow} + \hat{\Pi}_{\uparrow\uparrow} U \hat{\chi}_{\uparrow\downarrow} - \hat{\Pi}_{\uparrow\downarrow} U \hat{\chi}_{\uparrow\uparrow}, \quad (59)$$

$$\hat{\chi}_{\uparrow\downarrow} = -\hat{\Pi}_{\uparrow\uparrow} + \hat{\Pi}_{\uparrow\uparrow} U \hat{\chi}_{\uparrow\downarrow} - \hat{\Pi}_{\uparrow\downarrow} U \hat{\chi}_{\uparrow\uparrow}, \quad (60)$$

In the present numerical study, we calculate $\Delta\Pi_{\text{MT,AL}}(\alpha,\beta)$ only for region A in Fig. 3. Here we put $M = 3$ in the present section. Unfortunately, it is not easy to calculate all the elements of eqs. (49), (50) and (53) in the region A because of the huge computation time. Therefore, we calculate $\Delta\Pi_{\text{MT,AL}}(\alpha,\beta)$ only for $|\alpha - \beta| \leq 4$ in region A, and derive the static spin susceptibility $\hat{\chi}_{\text{GV+VC}}^s$ by solving eqs.(58) - (60) for region A+B.

Figure 10 show the local spin susceptibility given by GV^I -method [$\hat{\chi}^{Is}(i,i)$], GV-method [$\hat{\chi}^s(i,i)$], and GV+VC-method [$\hat{\chi}_{\text{GV+VC}}^s(i,i)$] for LSCO ($U = 4$, $n = 0.9$), respectively. At $i = (1,0)$, we see that $\hat{\chi}^{Is}(i,i)$ increases whereas $\hat{\chi}^s(i,i)$ decreases, as we have shown

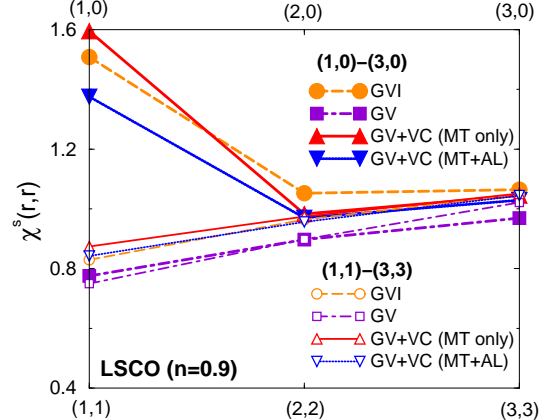


FIG. 10: (Color online) Local spin susceptibilities for $U = 4$ at $T = 0.02$ given by the GV, GV^I and GV+VC methods, respectively. $\chi^s(\mathbf{r},\mathbf{r})$ at $\mathbf{r} = (1,0)$ takes an enhanced value for both GV^I and GV+VC methods, whereas it decreases in the GV-method. We conclude that GV^I -method is as good as GV+VC-method.

in Fig. 6. Note that we have put $\Pi(i,j) = \Pi_I(i,j) = \Pi_{\text{GV+VC}}(i,j) = 0$ for $|i - j| > 4$ in deriving Fig. 10 to make comparison between different methods. Because of this fact, both $\hat{\chi}^{Is}(i,i)$ and $\hat{\chi}^s(i,i)$ in Fig. 10 are smaller than those in Fig. 6 for $U = 4$.

As shown in Fig. 10, $\hat{\chi}_{\text{GV+VC}}^s(i,i)$ at $i = (1,0)$ is strongly enhanced due to the VC's, to be comparable with $\hat{\chi}^{Is}(i,i)$. This enhancement is brought mainly by

the MT-term, whereas the AL-term slightly reduces the spin susceptibility. Therefore, the suppression of $\hat{\chi}^s$ in the GV -method, which is caused by the non-local self-energy correction $\delta\Sigma$, is almost recovered by the VC's. Therefore, the GV^I -method gives a reliable spin susceptibility around the impurity, because the total feedback effects almost cancel.

We comment that the superiority of the GV^I -method over the GV -method and the importance of the VC's would remind us of the GW approximation [54, 55, 56]. It is a first principle calculation for the self-energy, which is given by the convolution of the Green function G and the screened interaction W within the RPA. In the “fully self-consistent GW ”, both G and W are obtained self-consistently. In the GW_0 scheme, on the other hand, the self-energy is given by G and W_0 , where W_0 is the screened interaction without self-energy correction. Reference [54, 55, 56] shows that the descriptions of the bandwidth reduction and the satellite structure in the quasiparticle spectrum are satisfactory in the GW_0 , whereas results given by GW are much worse. This result clearly indicates the necessity of VC's in the GW .

VI. TRANSPORT PHENOMENA

In previous sections, we showed that the magnetic susceptibility is strongly enhanced around the impurity. This fact will cause the strong nonlocal change in the self-energy around the impurity, $\delta\Sigma$. In the present section, we will show that $\delta\Sigma$ gives rise to a huge residual resistivity at finite temperatures in nearly AF Fermi liquids, which is the most important finding in the present paper. Moreover, a small number of nonmagnetic impurities can cause a “Kondo-like” insulating behavior ($d\rho/dT < 0$) at low temperatures, when the system is very close to AF-QCP. Different from a conventional single-channel Kondo effect, the residual resistivity can be much larger than the value for s-wave unitary scattering. These findings naturally explain various long-standing problems on the transport phenomena in HTSC's, heavy fermion systems and organic superconductors.

A. T-matrix

First, we derive the expression for the t -matrix, $\hat{t}(\epsilon)$, which is defined as $\hat{G} = \hat{G}^0 + \hat{G}^0 \hat{t} \hat{G}^0$. Therefore, the t -matrix due to the impurity potential I at center $\mathbf{r} = (0, 0)$ is given by

$$t_{\alpha,\beta} = \sum_{n=1}^4 t_{\alpha,\beta}^{(n)}, \quad (61)$$

$$t_{\alpha,\beta}^{(1)} = (I + I^2 G_{0,0}) \delta_{\alpha,0} \delta_{\beta,0}, \quad (62)$$

$$t_{\alpha,\beta}^{(2)} = I \sum_{\nu}^A (G_{0,\nu} \delta\Sigma_{\nu,\beta} \cdot \delta_{\alpha,0} + \delta\Sigma_{\alpha,\nu} G_{\nu,0} \cdot \delta_{\beta,0}) \quad (63)$$

$$t = \begin{array}{c} \text{I} \\ \times \end{array} + \begin{array}{c} \text{I} \\ \times \end{array} \begin{array}{c} \text{G} \\ \text{---} \end{array} \begin{array}{c} \text{I} \\ \times \end{array} \quad (1)$$

$$+ \begin{array}{c} \times \\ \text{---} \end{array} \begin{array}{c} \text{---} \\ \text{---} \end{array} + \begin{array}{c} \text{---} \\ \text{---} \end{array} \begin{array}{c} \times \\ \text{---} \end{array} \quad (2)$$

$$+ \begin{array}{c} \text{---} \\ \text{---} \end{array} \begin{array}{c} \text{---} \\ \text{---} \end{array} \quad (3)$$

$$+ \begin{array}{c} \text{---} \\ \text{---} \end{array} \quad (4)$$

FIG. 11: Diagrammatic expression for the t -matrix given in eqs. (62)-(65).

$$t_{\alpha,\beta}^{(3)} = \sum_{\nu,\mu}^A \delta\Sigma_{\alpha,\nu} G_{\nu,\mu} \delta\Sigma_{\mu,\beta}, \quad (64)$$

$$t_{\alpha,\beta}^{(4)} = \delta\Sigma_{\alpha,\beta}, \quad (65)$$

where $t_{\alpha,\beta}^{(1)} \sim t_{\alpha,\beta}^{(4)}$ is schematically expressed in Fig. 11. α and β represent sites in region A.

Here, we derive the expression for the t -matrix in the limit $I \rightarrow \infty$. First, the second term of eq. (62) is rewritten as

$$I^2 G_{0,0} = I^2 G_{0,0}^I + I^2 \sum_{\alpha,\beta}^A G_{0,\alpha}^I \delta\Sigma_{\alpha,\beta} G_{\beta,0}^I + I^2 \sum_{\alpha,\beta,\gamma,\delta}^A G_{0,\alpha}^I \delta\Sigma_{\alpha,\beta} G_{\beta,\gamma} \delta\Sigma_{\gamma,\delta}^I G_{\delta,0}^I. \quad (66)$$

According to eq. (22),

$$I^2 G_{0,0}^I = -I - \frac{1}{G_{0,0}^0} + O(I^{-1}), \quad (67)$$

$$IG_{0,\alpha}^I = -\frac{G_{0,\alpha}^0}{G_{0,0}^0} + O(I^{-1}). \quad (68)$$

Thus, eq. (62) in the limit $I \rightarrow \infty$ is given by

$$I + I^2 G_{0,0} = -\frac{1}{G_{0,0}^0} + \sum_{\alpha\beta}^A \frac{G_{0,\alpha}^0 G_{\beta,0}^0}{(G_{0,0})^2} \times \left(\delta\Sigma_{\alpha,\beta} + \sum_{\gamma\delta}^A \delta\Sigma_{\alpha,\gamma} G_{\gamma,\delta} \delta\Sigma_{\delta,\beta} \right) \quad (69)$$

In the same way, eq. (63) in the limit $I \rightarrow \infty$ is given by

$$-\sum_{\delta}^A \frac{\delta\Sigma_{\alpha,\delta}}{G_{0,0}^0} \left(G_{\delta,0}^0 + \sum_{\xi\eta}^A G_{\delta,\xi} \delta\Sigma_{\xi,\eta} G_{\eta,0}^0 \right) \delta_{0,\beta} + \langle \alpha \leftrightarrow \beta \rangle. \quad (70)$$

Note that both eqs. (64) and (65) contain I only through $\delta\Sigma$, which does not diverge even when $I = \infty$.

To study the effect of the impurity on the transport phenomena, we take the average of the t-matrix with respect to the position of the impurity. The obtained result is

$$T_l \equiv \sum_{\alpha}^A t_{l+\alpha, \alpha} = -\frac{1}{G_{0,0}^0} \left(1 - \frac{1}{G_{0,0}^0} \sum_{\alpha \beta}^A D_{0,\alpha}^0 (\delta_{\alpha,\beta} + D_{\alpha,\beta}) G_{\beta,0}^0 \right) \delta_{l,0} \quad (71)$$

$$- \frac{2}{G_{0,0}^0} \sum_{\alpha}^A D_{0,\alpha}^0 (\delta_{\alpha,l} + D_{\alpha,l}) \quad (72)$$

$$+ \sum_{\alpha \beta \gamma}^A \delta \Sigma_{l+\alpha, \beta} G_{\beta, \gamma} \delta \Sigma_{\gamma, \alpha} \quad (73)$$

$$+ \sum_{\alpha}^A \delta \Sigma_{l+\alpha, \alpha}, \quad (74)$$

where eqs. (71), (72), (73) and (74) come from eqs. (62), (63), (64) and (65), respectively. $D_{\alpha,\beta}^0$ is given in eq. (31). Similarly, $D_{\alpha,\beta}$ is defined as

$$D_{\alpha,\beta} = \sum_{\gamma}^A G_{\alpha,\gamma} \delta \Sigma_{\gamma,\beta} = \sum_{\gamma}^A \delta \Sigma_{\beta,\gamma} G_{\gamma,\alpha}. \quad (75)$$

Note that $D_{\alpha,0} = D_{0,\alpha} = 0$ and $D_{\alpha,0}^0 = 0$, whereas $D_{0,\alpha}^0 \neq 0$. After the analytic continuation of $T_l(\epsilon_n)$, the quasiparticle damping rate (without the renormalization factor) due to the impurity is given by [57, 58]

$$\gamma_{\mathbf{k}}^{\text{imp}}(\epsilon) = \frac{n_{\text{imp}}}{N^2} \sum_l \text{Im} T_l(\epsilon - i\delta) e^{i\mathbf{k} \cdot \mathbf{r}_l}, \quad (76)$$

where n_{imp} is the density of impurities.

Figure 12 shows $\gamma_{\mathbf{k}}^{\text{imp}}(0)$ along the Fermi surface for LSCO at $T = 0.02$, obtained by GV^0 , GV and GV^I -methods. Here, we put $n_{\text{imp}} = 1$. $\gamma_{\mathbf{k}}^{\text{host}} = \text{Im} \Sigma_{\mathbf{k}}^0(-i\delta)$ in the host system given by the FLEX approximation. Filled square and triangular represents

$$\gamma_{\text{imp}}^0(\epsilon) \equiv -\text{Im} \frac{n_{\text{imp}}}{G_0^0(\epsilon - i\delta)}, \quad (77)$$

for $n_{\text{imp}} = 1$, where $G_0^0(\epsilon) = \frac{1}{N^2} \sum_{\mathbf{k}} G_{\mathbf{k}}^0(\epsilon)$ is the local Green function of the host. Equation (77) is a well-known expression for the quasiparticle damping rate due to s-wave unitary impurities. In fact, γ_{imp}^0 is derived from eq. (76) by putting $\delta \Sigma_{\alpha,\beta} = -\Sigma_{\alpha-\beta}^0 \cdot \delta_{\alpha\beta,0}$ in eqs. (71)-(74). When the particle-hole symmetry is approximately satisfied around the Fermi level, eq. (77) becomes $\gamma_{\text{imp}}^0(\epsilon) = n_{\text{imp}}/\pi N_{\text{host}}(\epsilon)$, where $N_{\text{host}}(\epsilon) = \text{Im} G_0^0(\epsilon - i\delta)/\pi$ is the DOS of the host system.

In each method (GV , GV^I and GV^0), $\gamma_{\mathbf{k}}^{\text{imp}}$ has a strong \mathbf{k} -dependence similar to $\gamma_{\mathbf{k}}^{\text{host}}$, as shown in Fig. 12.

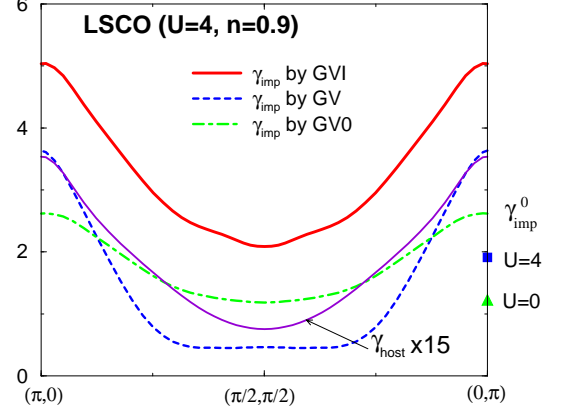


FIG. 12: (Color online) \mathbf{k} -dependence of $\gamma_{\mathbf{k}}^{\text{imp}}(0)$ per n_{imp} at $T = 0.02$, along the Fermi line. The shape of the Fermi line is shown in ref.[15]. $\gamma_{\text{host}} = \text{Im} \Sigma_{\mathbf{k}}^0(-i\delta)$ for the host system.

As a result, the structure of the “hot spot” and the “cold spot”, which are located around $(\pi/2, \pi/2)$ and $(\pi, 0)$ respectively, is not smeared out by strong non-magnetic impurities. This highly nontrivial result is brought by the \mathbf{k} -dependence of $\delta \Sigma_{\mathbf{k}}$. This finding strongly suggests that the enhancement of the Hall coefficient near the AF-QCP, which is brought by the strong back-flow (current vertex correction) around the cold spot [5, 15], does not decrease due to the strong impurities. In fact, the Hall coefficient for under-doped YBCO slightly increases by the doping of non-magnetic impurities [60].

On the other hand, in the case of weak impurities where the Born approximation is reliable, $\gamma_{\mathbf{k}}^{\text{imp}}$ should be almost \mathbf{k} -independent. Thus, the structure of the “hot/cold spots” will be smeared out by (large numbers of) weak non-magnetic impurities. By this reason, the enlarged Hall coefficient near the AF-QCP, which is brought by the back-flow around the cold spot, is reduced by weak non-magnetic impurities [61]. This theoretical result would be able to explain the reduction of R_H in CeCoIn₅ at very low temperatures [40, 41].

Another important finding is that $\gamma_{\mathbf{k}}^{\text{imp}}$ given by the GV^I -method becomes larger than $\gamma_{\mathbf{k}}^0$, due to the non-local scattering (non s-wave scattering) given by $\delta \Sigma$. Figure 13 shows $\gamma_{\mathbf{k}}^{\text{imp}}(0)$ for $n_{\text{imp}} = 1$ given by the GV^I -method, at $T = 0.02$ for LSCO, YBCO and NCCO. In both hole and electron-doped systems, the hot/cold spot structure in the host system remains even in the presence of impurities. The absolute value of $\gamma_{\mathbf{k}}^{\text{imp}}(0)$ increases drastically when the system is close to the AF-QCP, as shown in 13. This finding gives the explanation for the huge residual resistivity in metals near the AF-QCP, which has been a long-standing problem in strongly correlated electron systems. In contrast, $\gamma_{\mathbf{k}}^{\text{imp}}$ given by the GV^0 -method is comparable to $\gamma_{\mathbf{k}}^0$, because the enhancement of $\hat{\chi}^s$ around the impurity is not taken into account. Also, $\gamma_{\mathbf{k}}^{\text{imp}}$ by the GV -method is much smaller than $\gamma_{\mathbf{k}}^0$. This result will be an artifact of the GV -

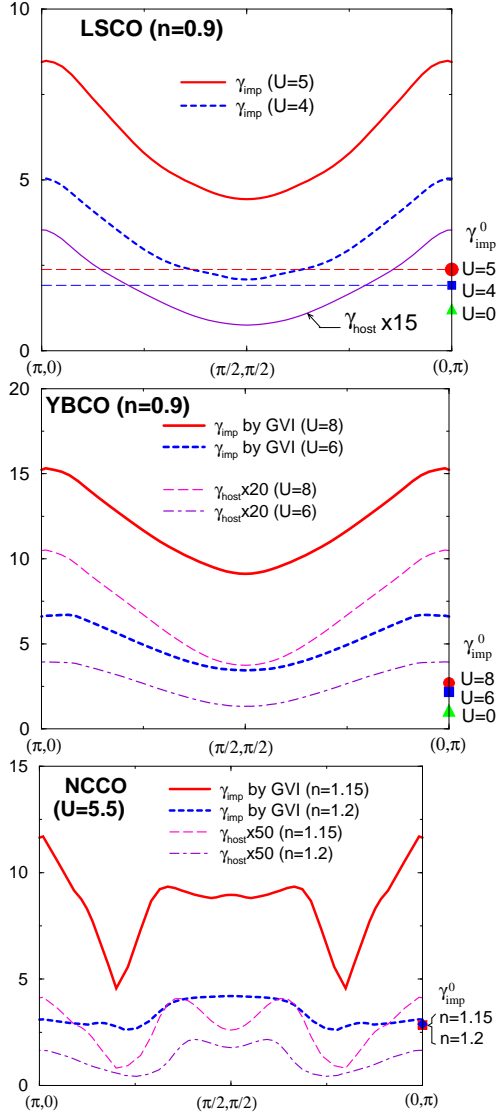


FIG. 13: (Color online) $\gamma_{\mathbf{k}}^{\text{imp}}(0)$ per n_{imp} at $T = 0.02$, along the Fermi line. They are given by the CV^I -method. Both $\gamma_{\mathbf{k}}^{\text{imp}}$ and γ_{host} show similar \mathbf{k} -dependence, which means that the hot/cold spot structure is maintained against the doping of strong nonmagnetic impurities. Moreover, $\gamma_{\mathbf{k}}^{\text{imp}}$ is much larger than $\gamma_{\mathbf{k}}^0$ when AF fluctuations are strong.

method, as discussed in §V.

Here, we examine the origin of the enhancement of $\gamma_{\mathbf{k}}^{\text{imp}}$ in more detail. Figure 14 shows $\gamma_{\mathbf{k}}^{\text{imp}(l)}$ ($l = 1 \sim 4$) for LSCO and YBCO, which represent contributions by eqs.(71)-(74), respectively. They are also expressed in Fig. 11. Note that $\gamma_{\mathbf{k}}^{\text{imp}} = \sum_{l=1}^4 \gamma_{\mathbf{k}}^{\text{imp}(l)}$. In both YBCO and LSCO, $\gamma_{\mathbf{k}}^{\text{imp}(2)}$ and $\gamma_{\mathbf{k}}^{\text{imp}(4)}$ give main contributions: The latter is dominant for YBCO, whereas $\gamma_{\mathbf{k}}^{\text{imp}(2)}$ is comparable to $\gamma_{\mathbf{k}}^{\text{imp}(4)}$ around $\mathbf{k} = (\pi/2, \pi/2)$ for LSCO. In both systems, $\gamma_{\mathbf{k}}^{\text{imp}(4)}$ grows drastically below $T = 0.02$

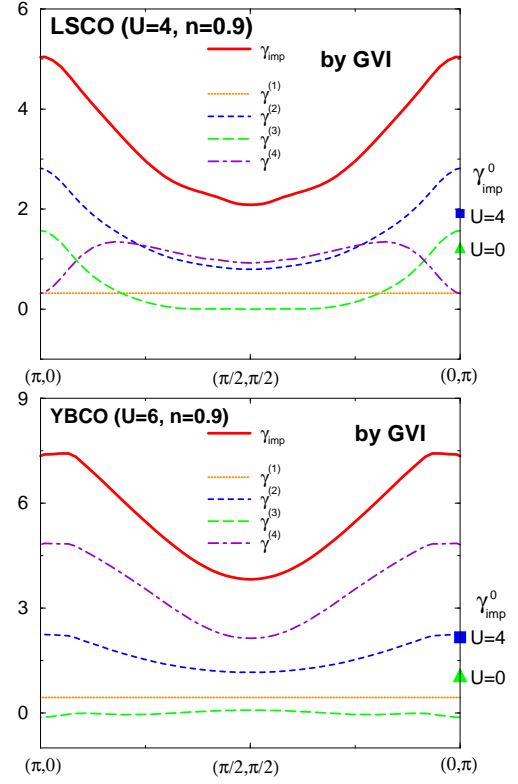


FIG. 14: (Color online) $\gamma_{\mathbf{k}}^{\text{imp}(l)}$ ($l = 1 \sim 4$) per n_{imp} at $T = 0.02$, along the Fermi line. They are given by the CV^I -method. They represent contributions by eqs.(71)-(74), respectively.

as U is increased. In the same way, $\gamma_{\mathbf{k}}^{\text{imp}(4)}$ takes a large value for NCCO at lower temperatures. This enhancement of $\gamma_{\mathbf{k}}^{\text{imp}(4)}$ at lower temperatures gives rise to the insulating behavior of the resistivity, as we will show later.

B. Resistivity

Here, we calculate the resistivity in nearly AF metals in the presence of strong impurities. Hereafter, we take account of the impurity effect only up to $O(n_{\text{imp}})$. In other words, we neglect the interference effect (e.g., the weak localization effect) which is given by the higher order terms with respect to n_{imp} . In fact, many anomalous impurity effects of HTSC in which we are interested are of the order of $O(n_{\text{imp}})$. For example, the residual resistivity in HTSC is proportional to the impurity concentration for $n_{\text{imp}} \lesssim 4\%$ [36]. Surprisingly, the residual resistivity per impurity increases drastically as the system approaches the half-filling. The relation $\Delta\rho \sim (4\hbar/e^2)n_{\text{imp}}/\delta$ holds in the under-doped region, which is n/δ times larger than the residual resistivity in 2D electron gas. ($\delta = |1 - n|$ is the carrier doping concentration.) Hereafter, we will explain this experimental fact based on the idea that the effective cross section of

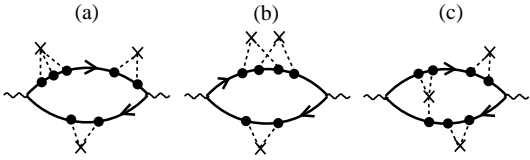


FIG. 15: Several diagrams for the conductivity in the presence of impurities. The residual resistivity $\Delta\rho$ given by type (a) and (c) diagrams is proportional to $O(n_{\text{imp}})$. On the other hand, $\Delta\rho$ given by type (b) diagrams is $O(n_{\text{imp}}^2)$. In the present study, we take only type (a) diagrams into account.

an impurity is enlarged due to many body effect near the AF-QCP.

The conductivity is given by the two-particle Green function; we show some diagrams in Fig. 15. Here, the cross represents the impurity potential, and the filled circle is the three point vertex due to the electron-electron correlation. In Fig. 15, the type (a) diagrams give the correction of the order of $O(n_{\text{imp}})$, whereas the type (b) diagrams are $O(n_{\text{imp}}^2)$ because they contain cross terms between different impurities [58]. Thus, we drop all the diagrams which contain cross terms. The type (c) diagrams, which contain current vertex corrections (CVC's) due to impurities, which are necessary to cancel the effect of forward scattering on the conductivity. However, we drop all the diagrams with CVC's for the simplicity of the calculations, which would be allowed for a qualitative discussion. We also drop the CVC due to the electron-electron correlation because it gives merely a small correction to the conductivity, as shown in ref. [15].

As a result, by neglecting the CVC's, the conductivity without and with impurities up to $O(n_{\text{imp}})$, σ_0 and σ_{imp} , are given by the following equations [57, 58, 59]:

$$\sigma_0 = e^2 \sum_{\mathbf{k}} \int \frac{d\epsilon}{\pi} \left(-\frac{\partial f}{\partial \epsilon} \right) |G_{\mathbf{k}}^0(\epsilon)|^2 v_{\mathbf{k}x}^2(\epsilon), \quad (78)$$

$$\sigma_{\text{imp}} = e^2 \sum_{\mathbf{k}} \int \frac{d\epsilon}{\pi} \left(-\frac{\partial f}{\partial \epsilon} \right) |\bar{G}_{\mathbf{k}}(\epsilon)|^2 v_{\mathbf{k}x}^2(\epsilon), \quad (79)$$

where $v_{\mathbf{k}x}(\epsilon) = \partial \epsilon_{\mathbf{k}} / \partial k_x + \text{Re} \Sigma_{\mathbf{k}}(\epsilon)$. $G_{\mathbf{k}}^0(\epsilon) = (\epsilon + \mu - \epsilon_{\mathbf{k}} - \Sigma_{\mathbf{k}}(\epsilon))^{-1}$ is the Green function obtained by the FLEX approximation without impurity. The averaged Green function in the presence of impurities, $\bar{G}_{\mathbf{k}}$, is given by

$$\bar{G}_{\mathbf{k}}(\epsilon - i\delta) = \left(\{G_{\mathbf{k}}^0(\epsilon - i\delta)\}^{-1} - i\gamma_{\mathbf{k}}^{\text{imp}}(\epsilon) \right)^{-1}. \quad (80)$$

Figure 16 shows the temperature dependences of the resistivities for LSCO, YBCO and NCCO obtained by the GV^I -method; $\rho_{\text{imp}} = 1/\sigma_{\text{imp}}$ for $n_{\text{imp}} = 0.02$. $\rho_0 = 1/\sigma_0$ is the resistivity without impurity. We see that the “residual resistivity” at finite T , which is the increment of resistivity due to impurity $\Delta\rho \equiv \rho_{\text{imp}} - \rho_0$, is approximately constant for a wide range of T , except for the abrupt increase at lower temperatures in YBCO and NCCO. $\Delta\rho$ grows as we enlarge U (YBCO, LSCO)

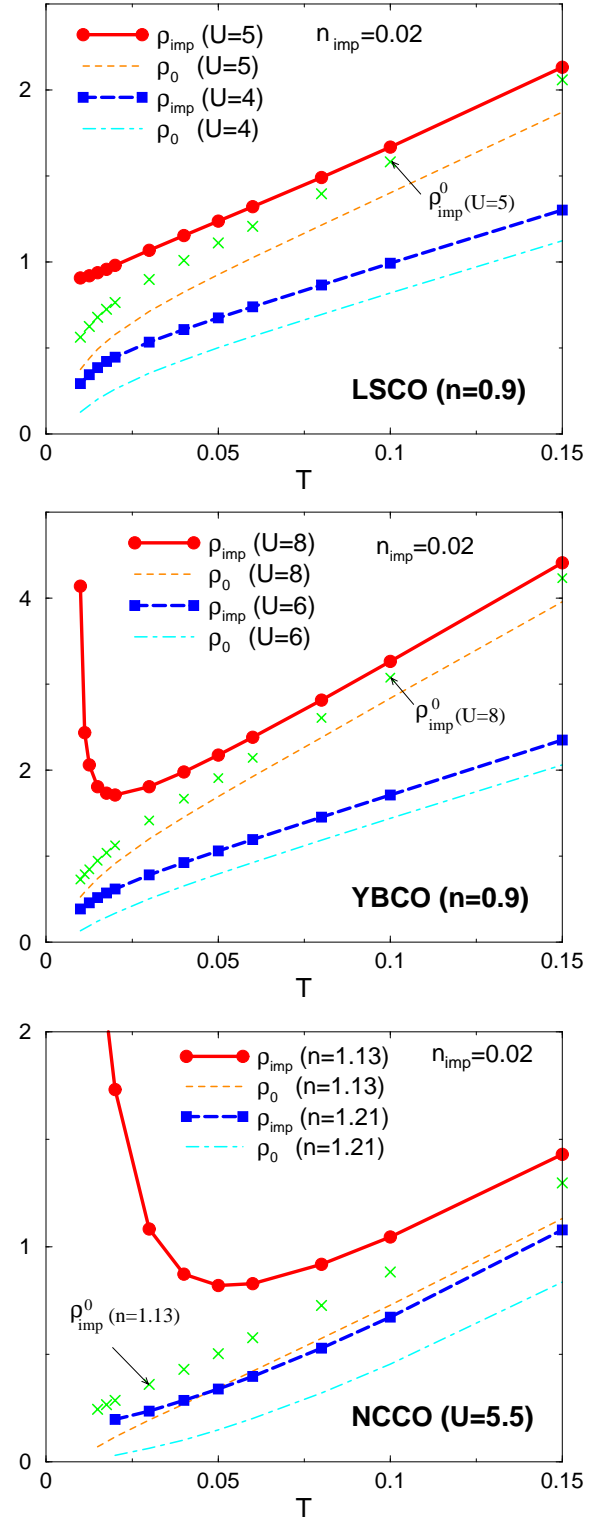


FIG. 16: (Color online) ρ_{imp} (ρ_{imp}^0) represents the resistivity for $n_{\text{imp}} = 0.02$ given by the GV^I -method (local scattering approximation). ρ_0 is the resistivity for the host system. At higher temperatures, the residual resistivity $\rho_{\text{imp}} - \rho_0$ is almost T -independent, and its value increases near the AF-QCP. At lower temperatures, the insulating behavior emerges in the close vicinity of the AF-QCP. $T = 0.1$ and $\rho = 1$ correspond to 400K and $250\mu\Omega\cdot\text{cm}$ for HTSC's, respectively.

or change the filling number n towards the half-filling (NCCO). This result comes from the fact that the scattering cross section of an impurity is enlarged by the non-local modulation of the self-energy, $\delta\Sigma$. In other words, non s-wave (elastic and inelastic) scatterings caused by $\delta\Sigma$ gives an anomalously large residual resistivity near the AF-QCP.

Figure 16 also shows that ρ_{imp}^0 derived from eq.(79) by replacing $\gamma_{\mathbf{k}}^{\text{imp}}(\epsilon)$ in eq.(80) with $\gamma_{\text{imp}}^0(\epsilon)$ which is momentum independent. We call it the “local scattering approximation” because non-s-wave impurity scattering processes caused by the nonlocal effect ($\delta\Sigma$) are dropped. In contrast to $\Delta\rho$, the doping dependences of $\Delta\rho^0 \equiv \rho_{\text{imp}}^0 - \rho_0$ is much moderate. Moreover, $\Delta\rho^0$ slightly decreases at low temperatures as $\gamma_{\mathbf{k}}$ becomes anisotropic: In fact, $\langle \frac{1}{\gamma_{\mathbf{k}} + \gamma_{\text{imp}}^0} \rangle^{-1} - \langle \frac{1}{\gamma_{\mathbf{k}}} \rangle^{-1} \ll \gamma_{\text{imp}}^0$ when $\gamma_{\mathbf{k}} (\gg \gamma_{\text{imp}}^0)$ is very anisotropic.

In each compound (YBCO, LSCO, NCCO), the average spacing between CuO₂-layers is about 6 Å. Using the relation $h/e^2 = 26\text{k}\Omega$, $\rho = 1$ in the present calculation corresponds to $250\mu\Omega\cdot\text{cm}$. As shown in fig. 16, residual resistivities for $n_{\text{imp}} = 0.02$ at $T = 0.05$ for LSCO ($U = 5$), YBCO ($U = 8$) and NCCO ($n = 1.13$) are 0.7, 1.0 and 0.8, respectively. They correspond to $175 \sim 250\mu\Omega\cdot\text{cm}$. These obtained values are close to the experimental residual resistivity in under-doped HTSC’s; $\Delta\rho \sim (4\hbar/e^2)n_{\text{imp}}/|1 - n|$ [36].

Another important findings is the insulating behavior ($d\rho_{\text{imp}}/dT < 0$) in YBCO and NCCO at lower temperatures. We also checked that a similar upturn is also observed in LSCO for $U = 6$. This insulating behavior of ρ_{imp} is caused by the steep increment of $\gamma_{\mathbf{k}}^{\text{imp}}$ at lower temperatures, which is mainly given by $\gamma_{\mathbf{k}}^{\text{imp}(4)} \propto \text{Im}\delta\Sigma(0)$. Therefore, the physical origin of this phenomenon is the strong inelastic scattering around the impurity. The obtained insulating behavior will be universal for systems with strong nonmagnetic impurities in the close vicinity of the AF-QCP. Actually, the upturn of ρ is widely observed in under-doped HTSC’s, both in hole-doped and electron-doped compounds [36, 43, 44, 45, 46]. The origin is not the weak localization as we explained in §I. Based on the present study, we expect that residual disorder will be the origin of the insulating behavior in HTSC’s.

In Fig. 17, we show that U dependences of $\Delta\rho$ and $\Delta\rho^0$ (per impurity) at $T = 0.02$ given by the GV^I -method, both for LSCO and YBCO. $\Delta\rho^0$ increases as U is raised, inversely proportional to the DOS given by the FLEX approximation, $N_{\text{host}}(0)$. We stress that $\Delta\rho$ increases drastically as U is raised, much faster than $\Delta\rho^0$ does. This prominent increment is derived from the strong inelastic scattering around the impurity, $\text{Im}\delta\Sigma(0)$. For comparison, we also show results given by the GV and GV^0 -methods in Fig. 17. $\Delta\rho_{[GV_0]}$ is close to $\Delta\rho^0$ because the enhancement of AF fluctuations around the impurity are not taken into account. Even worse, $\Delta\rho_{[GV]}$ decreases

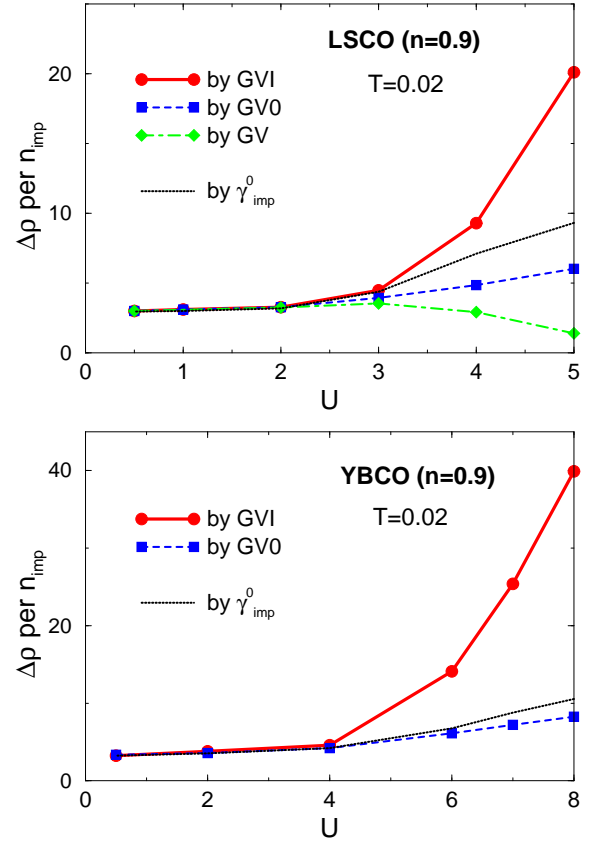


FIG. 17: (Color online) $\Delta\rho \equiv \rho_{\text{imp}} - \rho_0$ per n_{imp} at $T = 0.02$. $\Delta\rho$ given by the GV^I -method grows drastically as U increases, whereas $\Delta\rho$ by the GV -method gradually drops. Here, “by γ_{imp}^0 ” represents the residual resistivity by the local approximation, which slightly increases with U in proportion to $\gamma_{\text{imp}}^0 \propto 1/N_{\text{host}}(0)$.

for $U > 3$ in LSCO. This result should be an artifact of the GV -method, because it fails to reproduce the enhancement of spin fluctuations as explained in previous sections.

The prominent U -dependence of $\Delta\rho$ given by GV^I -method would corresponds to the pressure dependence of $\Delta\rho$ observed in κ -(BEDT-TTF)₄Hg_{2.89}Br₈, which stays near the AF-QCP at ambient pressure [42]. In this compound, $\Delta\rho$ decreases to one tenth of its original value by applying the pressure. Considering that the applied pressure makes U/W_{band} small, this experimental result is consistent with Fig. 17. We also note that the residual resistivity in heavy fermion systems near the magnetic instabilities frequently show prominent pressure dependence; $\Delta\rho$ takes a maximum value at the AF-QCP, and it decreases quickly as the system goes away from the AF-QCP. [37, 38, 39, 40, 41]. This experimental fact is well explained by Fig. 17.

Figure 18 shows the filling dependence of $\Delta\rho$ given by the GV^I -method at $T = 0.02$, which is above the upturn temperature of ρ for YBCO as recognized in Fig. 16. In

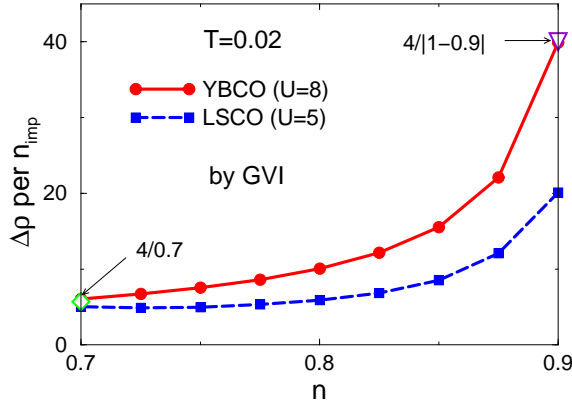


FIG. 18: (Color online) Filling-dependence of $\Delta\rho/n_{\text{imp}}$ given by the GV^I -method at $T = 0.02$. Origin of the huge $\Delta\rho$ in under-doped region is the short τ around impurities induced by strong AF fluctuations.

both LSCO and YBCO, $\Delta\rho$ increases drastically as n approaches unity, far beyond the s-wave unitary scattering value ($\sim 4/n$). The obtained result is consistent with experimental observations in HTSC's, where $\Delta\rho \sim \Delta\rho^0$ in the over-doped region, whereas $\Delta\rho \gg \Delta\rho^0$ in the under-doped region [36].

In the present calculation, we dropped all the CVC's for simplicity. As shown in ref. [15], ρ_0 without impurities is slightly enlarged by the CVC; effect of the CVC for ρ_0 is small because the origin of the resistivity is the large angle scattering due to AF fluctuations ($\mathbf{q} \approx (\pi, \pi)$). [In general, CVC's for the resistivity are important when small angle scatterings are dominant.] In the present calculation, the origin of the huge $\Delta\rho \propto \gamma_{\mathbf{k}}^{\text{imp}(4)}$ is also the AF fluctuations induced around the impurity. Therefore, we expect that obtained $\Delta\rho$ in this section is qualitatively reliable. On the other hand, CVC's play quite important roles on R_H , $\Delta\rho/\rho$ and ν [5]: It is an important future issue to study these transport coefficients in the presence of impurities by taking CVC's into account. Finally, we note that the obtained insulating behavior of ρ_{imp} might be under-estimated because the area of region A in the present numerical study ($M = 6 \sim 8$) would be not enough in the very close vicinity of the AF-QCP ($\xi_{\text{AF}} \gg 1$).

C. Decrease of the Hole Density n_h ($= |1 - n|$) around the Impurity, and Increase of $\Delta\rho$ at $T = 0$

Up to now, we have found that $\gamma_{\mathbf{k}}^{\text{imp}(4)}$ (and $\gamma_{\mathbf{k}}^{\text{imp}(2)}$) give the main contribution to the huge residual resistivity $\Delta\rho_{\text{imp}}$ at finite temperatures. However, $\gamma_{\mathbf{k}}^{\text{imp}(4)}(0) = 0$ at zero temperature because $\delta\Sigma_{l,m}(0)$ becomes a real function at $T = 0$. Therefore, it is highly nontrivial to predict the value of $\Delta\rho_{\text{imp}}$ at $T = 0$. On the other

hand, $\gamma_{\mathbf{k}}^{\text{imp}(1)}$, $\gamma_{\mathbf{k}}^{\text{imp}(2)}$ and $\gamma_{\mathbf{k}}^{\text{imp}(3)}$ could give an enlarged $\Delta\rho_{\text{imp}} \gg \Delta\rho_{\text{imp}}^0$ at zero temperatures, because they are finite even at $T = 0$.

Hereafter, we discuss the residual resistivity at $T = 0$. For simplicity, we assume an two-dimensional isotropic system with the dispersion $\epsilon_{\mathbf{k}} = \mathbf{k}^2/2m$. At $T = 0$, $\gamma_{\mathbf{k}}^{\text{imp}}$ is given by

$$\begin{aligned} \gamma_{\mathbf{k}}^{\text{imp}} &= n_{\text{imp}} \text{Im} T_{\mathbf{k}, \mathbf{k}} \\ &= n_{\text{imp}} \frac{2}{m} \sum_l \sin^2 \delta_l, \end{aligned} \quad (81)$$

where l represents the angular momentum with respect to the impurity potential ($l = 0, \pm 1, \pm 2, \dots$), and δ_l is the phase shift for channel l . If we drop the CVC, the resistivity at $T = 0$ is given by [58]

$$\rho_{\text{imp}} = \frac{4\hbar n_{\text{imp}}}{e^2 n} \sum_l \sin^2 \delta_l. \quad (82)$$

Here, $\sin^2 \delta_l$ is replaced with $\sin^2 \delta_l - \cos(\delta_l - \delta_{l+1}) \sin \delta_l \sin \delta_{l+1}$ if the CVC due to impurity is taken into account. On the other hand, the number of localized electrons around the impurity, Δn_{tot} , in an isotropic 2D system is given by [62]

$$\Delta n_{\text{tot}} = \frac{2}{\pi} \sum_l \delta_l. \quad (83)$$

Thus, the residual resistivity at $T = 0$ will grows as the number of electrons in bound states increases.

YBCO

T	0.01	0.015	0.02	0.05
$100 \times \Delta n(1, 0)$	6.15	1.50	1.06	0.60
Δn_{tot}	2.86	0.334	0.190	0.052
α_{St}	0.9968	0.9950	0.9932	0.9807

NCCO

T	0.02	0.025	0.03	0.06
$100 \times \Delta n(1, 0)$	-3.84	-3.12	-2.78	-2.13
Δn_{tot}	-1.52	-0.897	-0.639	-0.254
α_{St}	0.9965	0.9958	0.9948	0.9839

TABLE I: Temperature dependences of $\Delta n(1, 0)$, Δn_{tot} and the Stoner factor $\alpha_{\text{St}} = \max_{\mathbf{q}} U\Pi_{\mathbf{q}}^0(0)$.

Table I represent $\Delta n(1, 0) \equiv n(1, 0) - n$ and $\Delta n_{\text{tot}} \equiv \sum_{\mathbf{r}} \Delta n(\mathbf{r})$ for both YBCO ($n = 0.9$, $U = 8$) and NCCO ($n = 1.13$, $U = 5.5$). We see that the number of electron at $\mathbf{r} = (1, 0)$ approaches the half filling ($n = 1$) at low temperatures for both YBCO and NCCO. Moreover, Δn_{tot} increases (decreases) prominently in YBCO (NCCO) as T decreases. This result suggests that the residual resistivities at $T = 0$ will be larger than ρ_{imp}^0 in the vicinity of the AF-QCP.

Finally, we discuss why $n(1,0)$ approaches unity and Δn_{tot} increases (decreases) in hole-doped (electron-doped) systems. In the FLEX approximation, the thermodynamic potential Ω in a uniform system is given by [63]

$$\begin{aligned} \Omega = & -T \sum_{\mathbf{q}, l} \text{Tr} [\Sigma G + \ln(-[G^0]^{-1} + \Sigma)] \\ & + T \sum_{\mathbf{q}, l} \text{Tr} \left[\frac{3}{2} \ln(1 - U\Pi^0) + \frac{1}{2} \ln(1 + U\Pi^0) \right. \\ & \left. + U\Pi^0 + U^2[\Pi^0]^2 \right]. \end{aligned} \quad (84)$$

As we explained, the AF fluctuations are enhanced around the impurity. This effect would be expressed by increasing $\Pi^0(\mathbf{q}, \omega_l)$ in eq. (84) by $\Delta\Pi^0$ (> 0), or U by ΔU (> 0). According to eq. (84),

$$\frac{\partial\Omega}{\partial U} \approx -\frac{3}{2}T \sum_{\mathbf{q}, l} \Pi^0(\mathbf{q}, \omega_l) (1 - U\Pi^0(\mathbf{q}, \omega_l))^{-1}, \quad (85)$$

in the case of $1 - U\Pi^0(\mathbf{Q}, 0) \ll 1$. In deriving (85), we used the fact that the implicit derivative through Σ vanishes because of the stationary condition $\delta\Omega/\delta\Sigma = 0$ in the conserving approximation [6, 64]. According to eq.(85), we obtain

$$\begin{aligned} \frac{\partial n}{\partial U} &= -\frac{\partial}{\partial U} \left(\frac{\partial\Omega}{\partial\mu} \right) \\ &= \frac{3}{2}T \sum_{\mathbf{q}, l} \frac{1}{(1 - U\Pi^0(\mathbf{q}, \omega_l))^2} \frac{\partial\Pi^0(\mathbf{q}, \omega_l)}{\partial\mu}. \end{aligned} \quad (86)$$

As a result, the electron density n around the impurity, where $\Delta U > 0$ is satisfied as mentioned above, increase (decreases) when $\partial\Pi(\mathbf{Q}, 0)/\partial\mu$ is positive (negative). Therefore, we conclude that Δn_{tot} will increase (decrease) in hole-doped (electron-doped) systems, as recognized by numerical results given by the GV^I -method.

VII. DISCUSSIONS

A. Summary of the Present Work and Future Problems

The present study reveals that a single impurity strongly affects the electronic states in a wide area around the impurity in the vicinity of the AF-QCP. For this purpose, we developed the GV^I -FLEX method, which is a powerful method to study the impurity effect in strongly correlated systems. The GV^I method is much superior to the GV , which is a fully self-consistent FLEX approximation. Using the GV^I method, characteristic impurity effects in under-doped HTSC's are well explained in a unified way, without introducing any exotic mechanisms assuming the breakdown of the Fermi liquid state. The main numerical results are shown in Fig. 5 (local DOS

around the impurity site), Figs. 6-8 (local and staggered susceptibilities), and Figs. 16-18 (resistivity in the presence of impurities). Qualitatively, these obtained numerical results are very similar for YBCO, LSCO and NCCO. Therefore, novel impurity effects in nearly AF metals revealed by the present work would be universal.

Based on the GV^I method, we found that both local and staggered susceptibilities are prominently enhanced around the impurity site, as shown in Figs. 6 and 6. Especially, a nonmagnetic impurity causes a Curie-like spin susceptibility, $\mu_{\text{eff}}^2/3T$. The GV^I -method gives $\mu_{\text{eff}} \approx 0.74\mu_B$ for LSCO ($n = 0.9$, $U = 5$), shown in Figs. 8. Note that $\mu_{\text{eff}} \sim 1\mu_B$ in $\text{YBa}_2\text{Cu}_3\text{O}_{6.66}$ ($T_c \approx 60K$). We also found that the quasiparticle damping rate takes a huge value around the impurity, owing to the enhanced AF fluctuations. By this reason, the local DOS at the Fermi level is strongly suppressed around the impurity site, which forms a so-called "Swiss cheese structure" as shown in Fig. 19. Its radius is about the AF correlation length of the host, ξ_{AF} , which is about $3 \sim 4a$ (a being the lattice spacing) in slightly under-doped HTSC's at $T = 0.02$. We guess that Swiss cheese holes stay in a normal state even below T_c , because of the extremely short quasiparticle lifetime there. In fact, the residual specific heat ($T \ll T_c$) induced by an impurity becomes very large in under-doped systems [50]. This experimental fact will be explained in our future study based on the GV^I -method [61].

Near the AF-QCP, the short quasiparticle lifetime inside the Swiss cheese hole gives rise to a huge residual resistivity $\Delta\rho$, as shown in Figs. 16-18. In the under-doped region, $\Delta\rho$ grows far beyond the s-wave unitary scattering limit $\sim (4\hbar/e^2)n_{\text{imp}}/n$. We find that $\Delta\rho$ is almost T -independent for a wide range of temperature, and it increases drastically as the system approaches the AF-QCP. This result is consistent with experiments for HTSC's. The obtained value of $\Delta\rho$, $175 \sim 250\mu\Omega\cdot\text{cm}$ for $n_{\text{imp}} = 0.02$, are recognized in under-doped HTSC's [36]. Furthermore, in the close vicinity of the AF-QCP, the resistivity given by the GV^I -method shows the "Kondo-like" insulating behavior ($d\rho/dT < 0$) under the presence of nonmagnetic impurities with low concentration ($\sim 2\%$). This surprising result would explain the "upturn of resistivity" which is frequently observed in under-doped HTSC's, by assuming the existence of residual disorders. The mechanism of this insulating behavior had been a long-standing unsolved issue in under-doped HTSC's. Different from a conventional single-channel Kondo effect, the residual resistivity given by the GV^I -method grows far beyond $(4\hbar/e^2)n_{\text{imp}}/n$.

We stress that that $\gamma_{\mathbf{k}}^{\text{imp}}$ given by the GV^I -method has strong \mathbf{k} -dependence, so the structure of "hot/cold spots" is maintained against impurity doping. This result could be examined by the ARPES measurements. We also comment that the CVC's due to spin fluctuations cause a finite "residual resistivity", if we define it as the extrapolated value at $T = 0$, even in the absence of impurities [15]. We have to take this fact into account

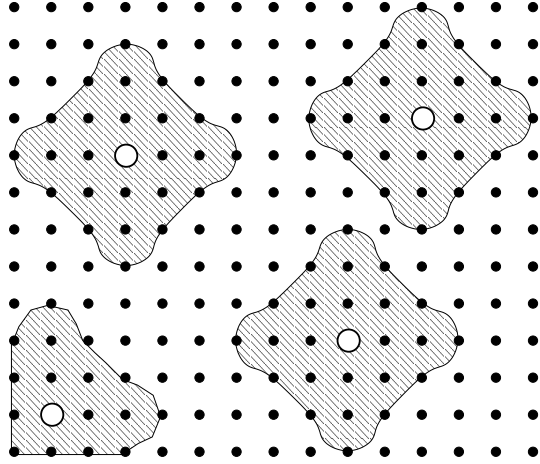


FIG. 19: Swiss cheese structure induced by nonmagnetic impurities ($n_{\text{imp}} = 0.021$) denoted by open circles, which replace Cu sites randomly. In the shadow area, both local and staggered spin susceptibilities are enhanced, and the quasiparticle lifetime is depressed. The radius of the Swiss cheese hole is $\sim \xi_{\text{AF}}$.

in analysing experimental data.

In the FLEX approximation, the AF-order (in the RPA) is suppressed by thermal and quantum fluctuations, which is expressed by Σ^0 . In the GV^I -method, the reduction of fluctuations around the impurity site gives rise to the enhancement of susceptibility. However, this mechanism is absent in the RPA. Therefore, the enhancement of susceptibility is tiny within the RPA. In addition, in the GV^I -method, the spin (charge) susceptibility $\chi^{\text{Is(c)}}$ contains the self-energy correction by U 's and that by I 's are treated on the same footing, whereas the cross term $\delta\Sigma$ is dropped because it will be cancelled out by VC's in large part. On the other hand, χ^{RPA} given by the RPA contains only self-energy correction by I 's [24, 25, 26]. This equal footing treatment of the correlation effect and the impurity effect in the GV^I -method would be the reason for the superiority of this method.

In future, we will study the transport phenomena by taking the current vertex corrections (CVC) accurately, in order to solve the impurity effect on various transport coefficients in HTSC's and in related systems. [61]. We will also study the superconducting state around a nonmagnetic impurity in under-doped HTSC's [61], to explain experimental observations given by STM/STS measurements [48, 51, 52]. As for HF systems and in organic metals, the strength of residual impurity (or disorder) potential would be comparable with bandwidth W_{band} . Therefore, we have to study to what extent the obtained results in the present paper (for $I = \infty$) hold in the case of $I \sim W_{\text{band}}$.

B. Possibility of the Impurity-Induced Magnetic Order

In the GV^I -method, the self-energy for the host system is given by the FLEX approximation, which cannot be applicable for heavily under-doped systems near the Mott insulating state. However, FLEX approximation gives qualitatively reliable results for slightly under-doped region ($|1-n| \sim 0.1$) to over-doped region [8, 9, 10, 11, 15]. To obtain quantitatively reliable results for under-doped region, vertex correction (VC) for the self-energy will be necessary, as indicated by ref. [65]. The pseudo-gap phenomena under T^* are well reproduced by the FLEX+ T -matrix approximation, where self-energy correction due to strong superconducting (SC) fluctuations are taken into account [1, 5, 12, 18]. By taking the CVC due to SC fluctuations into consideration, anomalous transport phenomena in HTSC's under T^* (e.g., prominent enhancement of the Nernst coefficient) are well understood in a unified way [5, 18].

One of the merits of the FLEX approximation is that the Mermin-Wagner theorem with respect to the magnetic instability is satisfied. In fact, previous numerical studies based on the FLEX report that no SDW-order emerges in two dimensional systems at finite T . In Appendix A, we offer an strong analytical evidence that the FLEX approximation satisfies the Mermin-Wagner theorem. Also, the GV^I -method does not predict any SDW-order in two dimensional systems with single impurities, at least for model parameters studied in the present paper. However, when the concentration of impurities is finite, Swiss cheese holes will overlap when ξ_{AF} exceeds the mean distance between impurities (l). Therefore, a SDW-order or a spin-glass order would happen when $\xi_{\text{AF}} > l$. In fact, in Zn-doped YBCO, the freezing of local moments due to Zn was observed by μ -SR study at very low temperatures [66]. Note that impurity induced AF order occurs in two-leg ladder Heisenberg models [67].

C. Comments on Related Theoretical Works

Here, we discuss the impurity effect on the electronic states of the “host system”. We did not study this effect because it is higher order effect with respect to n_{imp} . In Zn-doped $\text{YBa}_2\text{Cu}_4\text{O}_8$, Ihot et al. measured $^{63}\text{Cu } 1/T_1T$ in the host system (i.e., away from the Zn sites) [68], and found that the host AF fluctuations above T^* are reduced by a few percent doping of Zn. They suggest that the localization effect would be the origin of this reduction.

Based on the FLEX approximation (GV -method in the present paper), authors of ref. [69] studied the impurity effect on the electronic state by neglecting the \mathbf{k} -dependence of the self-energy. They reported that the AF fluctuation in the host system is depressed by impurities, which seems to be consistent with ref. [68]. As we have shown however, the GV -method fails to reproduce

correct electronic states around the impurity: In fact, both the Curie like $\Delta\chi^s$ as well as the huge $\Delta\rho$ are satisfactorily reproduced only by the GV^I -method. We note that $\rho(T)$ in HTSC shows a nearly parallel shift by the impurity doping, which means that the inelastic scattering in the host system is independent of impurities. This fact would suggest that the AF fluctuations in the host system is unchanged, in contrast to the NMR result [68]. It would be an important issue to understand these two experimental facts consistently.

Next, we comment that Miyake et al. have intensively studied the impurity effects near QCP [70]. They found that $\Delta\rho$ due to weak impurities (Born scattering) is enlarged when the charge fluctuations are developed. Their analysis corresponds to GV^0 -method since the susceptibility is assumed to be independent of impurities. In contrast, the present work based on GV^I -method shows that the $\Delta\rho$ due to strong impurities increases near the AF-QCP, which originates from the enhancement of χ^{Is} around the impurity. We note that $\chi_{\text{FLEX}}^c \equiv dn/d\mu$ is less than half of its non-interacting value in the present range of parameters. In analysing experiments, we have to consider carefully which kind of criticality may occur in the compound under consideration.

Finally, we explain previous studies on disordered Hubbard model based on the dynamical-mean-field-theory (DMFT) in the $d = \infty$ limit [71, 72, 73], and we make comparison with the present study. In the DMFT, the local-moment formation is found when strong hopping disorders (offdiagonal disorders) exist [71]. Also, it is found that the Néel temperature increases due to weak onsite disorders (diagonal disorders); $I < U$ [72]. However, a local-moment formation outsside of the impurity and a huge residual resistivity, which are realized in HTSC's, cannot be explained by the DMFT. For this purpose, a nonlocal modulation of the self-energy around the impurity have to be taken into account, which is possible in the GV^I -method.

Acknowledgments

We would like to thank Y. Ando, Y. Matsuda, T. Shibauchi, T. Sekitani, M. Ido, M. Oda, N. Momono, H. Taniguchi, M. Sato, K. Yamada, D.S. Hirashima, Y. Tanaka, M. Ogata, Y. Yanase and S. Onari for valuable comments and discussions.

APPENDIX A: MERMIN-WAGNER THEOREM IN 2D ELECTRON SYSTEMS

The Mermin-Wagner (M-W) theorem states that any magnetic instabilities are absent at finite T in 2D systems. Actually, the SCR theory satisfies the M-W theorem [2]. As for the FLEX approximation, however, the M-W theorem had been recognized only by numerical studies. In this appendix, we present a strong analytical evidence that the FLEX-type self-consistent spin fluctuation theory satisfies the M-W theorem.

Here we introduce the phenomenological expression for the dynamical spin susceptibility as

$$\chi_{\mathbf{q}}(\omega) = \frac{\chi_{\mathbf{Q}}}{1 + \xi_{\text{AF}}^2(\mathbf{q} - \mathbf{Q})^2 - i\omega/\omega_{\text{sf}}}, \quad (\text{A1})$$

where ξ_{AF} is the AF correlation length. \mathbf{Q} is one of the nesting vectors which minimize $|\mathbf{q} - \mathbf{Q}|$. Apparently, $\chi_{\mathbf{q}}(0) = \chi_{-\mathbf{q}}(0)$. Both $\chi_{\mathbf{Q}}$ and ω_{sf}^{-1} are proportional to ξ_{AF}^2 in the FLEX approximation.

When the system is very close to the AF phase at finite temperatures where $\omega_{\text{sf}} \gg T$ is satisfied, the self-energy within the scheme of the FLEX approximation is given by

$$\begin{aligned} \Sigma_{\mathbf{k}}(i\omega_n) &\approx T \sum_{\mathbf{q}} G_{\mathbf{k}+\mathbf{q}}(i\omega_n) \chi_{\mathbf{q}}(0) \\ &\approx G_{\mathbf{k}+\mathbf{Q}}(i\omega_n) A \end{aligned} \quad (\text{A2})$$

$$A = T \frac{3U^2}{2} \sum_{\mathbf{q}} \chi_{\mathbf{q}}(0) \quad (\text{A3})$$

where the static approximation is applied, which will offer the upper limit of T_N . A diverges as $T \rightarrow T_N$ in proportion to $T \ln \xi_{\text{AF}}$. Especially, $A = \infty$ at $T = T_N(> 0)$. On the other hand, A is finite even at $T = T_N$ in 3D systems. According to eq.(A2),

$$\begin{aligned} \Sigma_{\mathbf{k}}(i\omega_n) &= \frac{A}{i\omega_n - \epsilon_{\mathbf{k}+\mathbf{Q}} - \Sigma_{\mathbf{k}+\mathbf{Q}}(i\omega_n)} \\ &= \frac{A}{i\omega_n - \epsilon_{\mathbf{k}+\mathbf{Q}} - \frac{A}{i\omega_n - \epsilon_{\mathbf{k}} - \Sigma_{\mathbf{k}}(i\omega_n)}} \end{aligned} \quad (\text{A4})$$

Equation (A4) can be solved analytically. Considering $\Sigma_{\mathbf{k}}(\omega) = 0$ when $A = 0$, the self-energy and the Green function for real frequencies are given by

$$\Sigma_{\mathbf{k}}(\omega) = \frac{1}{2}(\omega - \epsilon_{\mathbf{k}}) - \text{sgn}(\omega - \epsilon_{\mathbf{k}}) \frac{1}{2} \sqrt{(\omega - \epsilon_{\mathbf{k}})^2 - 4A \frac{\omega - \epsilon_{\mathbf{k}}}{\omega - \epsilon_{\mathbf{k}+\mathbf{Q}}}} \quad (\text{A5})$$

$$G_{\mathbf{k}}(\omega) = \left(\frac{1}{2}(\omega - \epsilon_{\mathbf{k}}) + \text{sgn}(\omega - \epsilon_{\mathbf{k}}) \frac{1}{2} \sqrt{(\omega - \epsilon_{\mathbf{k}})^2 - 4A \frac{\omega - \epsilon_{\mathbf{k}}}{\omega - \epsilon_{\mathbf{k}+\mathbf{Q}}}} \right)^{-1} \quad (\text{A6})$$

One can check that $\omega \cdot \text{Im}\Sigma_{\mathbf{k}}(\omega) \leq 0$. This is not a Fermi liquid because the renormalization factor z is zero (owing

to the static approximation). Hereafter, we assume $\epsilon_{\mathbf{k}} = 2t(\cos k_x + \cos k_y)$ at half filling ($n = 1$), that is, both the perfect nesting and the particle-hole symmetry exist. Apparently, $Q = (\pi, \pi)$, $\epsilon_{\mathbf{k}+Q} = -\epsilon_{\mathbf{k}}$, and $\mu = 0$. The irreducible susceptibility at $\mathbf{q} = \mathbf{Q}$ and $\omega = 0$ is given by

$$\Pi_{\mathbf{Q}}(0) = -\sum_{\mathbf{k}} \int \frac{d\omega}{2\pi} \text{th} \frac{\omega}{2T} \text{Im}\{G_{\mathbf{k}+\mathbf{Q}}^R(\omega)G_{\mathbf{k}}^R(\omega)\} \quad (\text{A7})$$

According to eq. (A6),

$$G_{\mathbf{k}+\mathbf{Q}}(\omega)G_{\mathbf{k}}(\omega) = \left(\frac{1}{4}(\omega^2 - \epsilon_{\mathbf{k}}^2) + \frac{1}{2}\text{sgn}(\omega^2 - \epsilon_{\mathbf{k}}^2)\sqrt{g_{\mathbf{k}}(\omega)} + \frac{1}{4}\text{sgn}(\omega^2 - \epsilon_{\mathbf{k}}^2)|\omega^2 - \epsilon_{\mathbf{k}}^2 - 4A| \right)^{-1} \quad (\text{A8})$$

$$g_{\mathbf{k}}(\omega) = (\omega^2 - \epsilon_{\mathbf{k}}^2)(\omega^2 - \epsilon_{\mathbf{k}}^2 - 4A) \quad (\text{A9})$$

$g_{\mathbf{k}}(\omega)$ is negative when $|\epsilon_{\mathbf{k}}| < |\omega| < \sqrt{\epsilon_{\mathbf{k}}^2 + 4A}$. Apparently, the integrand in eq.(A7) is finite only when $g_{\mathbf{k}}(\omega) < 0$.

$$-\text{Im}\{G_{\mathbf{k}+\mathbf{Q}}(\omega)G_{\mathbf{k}}(\omega)\} = -\text{Im}\{ (A + \frac{i}{2}\sqrt{-g_{\mathbf{k}}(\omega)})^{-1} \} < \frac{1}{2A} \quad \text{for } g_{\mathbf{k}}(\omega) < 0 \quad (\text{A10})$$

$$= 0 \quad \text{for } g_{\mathbf{k}}(\omega) > 0 \quad (\text{A11})$$

According to eq.(A7), in the case of $\sqrt{A} \gg W_{\text{band}}$,

$$\Pi_{\mathbf{Q}}(0) \sim O(A^{-1/2}) \quad (\text{A12})$$

Note that $\text{Im}G_{\mathbf{k}}(\omega)$ is non-zero when $g_{\mathbf{k}}(\omega) < 0$, and one can check that $\int_{-\infty}^{\infty} d\omega \text{Im}G_{\mathbf{k}}^R(\omega) = -\pi$ for any A by MATHEMATICA. Considering that $\chi_{\mathbf{Q}}(0) = \Pi_{\mathbf{Q}}(0)/(1 - U\Pi_{\mathbf{Q}}(0))$ in the FLEX approximation, eq. (A12) means that $\chi_{\mathbf{Q}}(0)$ approaches to zero as $T \rightarrow T_N$ (because $A \rightarrow \infty$ in the case of $T_N > 0$) in 2D systems. Equation (A12) suggests that $\xi_{\text{AF}} \propto e^{1/T}$ when the ground state is a ordered state.

As a result, T_N cannot take a finite value in the two dimensional model with perfect nesting at half filling, which is the most likely to cause the magnetic instability. Therefore, the present analysis gives a compelling

evidence the the FLEX approximation satisfies the M-W theorem for general 2D systems.

Here we rewrite A as $A' + A''$, where $A' = T \frac{3U^2}{2} \sum_{\mathbf{q}} \chi_{\mathbf{q}}(0)$, and q_c is a cutoff momentum.

Then, A'' is a smooth function around the AF-QCP. When $T > \xi_{\text{AF}}^{-2} + q_c^2$, A' will be the number of free bosons (magnons) with energy $\epsilon_{\mathbf{q}} = q^2$ within the radius of q_c at the chemical potential $\mu = -\xi_{\text{AF}}^{-2}$. Thus, a magnetic instability ($\xi_{\text{AF}} \rightarrow \infty$) corresponds to the Bose-Einstein condensation of magnons ($\mu = 0$). Therefore, a meaningful correspondence between the M-W theorem and the absence (presence) of the Bose-Einstein condensation in 2D (3D) systems is recognized.

[1] Y. Yanase, T. Jujo, T. Nomura, H. Ikeda, T. Hotta and K. Yamada: *Phys. Rep.* **387** (2003) 1.
[2] T. Moriya and K. Ueda: *Adv. Physics* **49** (2000) 555.
[3] D. Manske, *Theory of Unconventional Superconductors: Cooper-Pairing Mediated By Spin Excitations* (Springer 2004, Berlin).
[4] P. Monthoux and D. Pines: *Phys. Rev. B* **47** (1993) 6069.
[5] H. Kontani and K. Yamada: *J. Phy. Soc. Jpn.* **74** (2005) 155.
[6] N. E. Bickers and S. R. White: *Phys. Rev. B* **43** (1991) 8044.
[7] P. Monthoux and D. J. Scalapino, *Phys. Rev. Lett.* **72** (1994) 1874.
[8] T. Takimoto and T. Moriya: *J. Phy. Soc. Jpn.* **66** (1997) 2459.
[9] S. Koikegami, S. Fujimoto and K. Yamada: *J. Phy. Soc. Jpn.* **66** (1997) 1438.
[10] S. Wermbter: *Phys. Rev. B* **55** (1997) R10149.
[11] D. Manske, I. Eremin and K.H. Bennemann: *Phys. Rev. B* **67** (2003) 134520.
[12] T. Dahm, D. Manske and L. Tewordt: *Europhys. Lett.* **55** (2001) 93.
[13] J. Takeda, T. Nishikawa, and M. Sato: *Physica C* **231** (1994) 293.
[14] T. Kimura, S. Miyasaka, H. Takagi, K. Tamasaku, H. Eisaki, S. Uchida, K. Kitazawa, M. Hiroi, M. Sera, and N. Kobayashi: *Phys. Rev. B* **53** (1996) 8733.
[15] H. Kontani, K. Kanki and K. Ueda: *Phys. Rev. B* **59** (1999) 14723, K. Kanki and H. Kontani: *J. Phys. Soc. Jpn.* **68** (1999) 1614.
[16] H. Kontani: *J. Phys. Soc. Jpn.* **70** (2001) 1873.
[17] H. Kontani: *J. Phys. Soc. Jpn.* **70** (2001) 2840.
[18] H. Kontani: *Phys. Rev. Lett.* **89** (2003) 237003.
[19] W. Ziegler, D. Poilblanc, R. Preuss, W. Hanke, and D. J. Scalapino: *Phys. Rev. B* **53** (1996) 8704.
[20] D. Poilblanc, D.J. Scalapino, and W. Hanke: *Phys. Rev. Lett.* **72** (1994) 884.
[21] N. Bulut, D. Hone, D.J. Scalapino, and E.Y. Loh: *Phys.*

Rev. Lett. **62** (1989) 2192.

[22] A.W. Sandvik, E. Dagotto, and D.J. Scalapino: Phys. Rev. B **56** (1997) 11701.

[23] H. Tsuchiura, Y. Tanaka, M. Ogata, and S. Kashiwaya: Phys. Rev. B **64** (2001) 140501(R).

[24] N. Bulut: Physica C **363** (2001) 260.

[25] N. Bulut: Phys. Rev. B **61** (2000) 9051.

[26] Y. Ohashi: J. Phys. Soc. Jpn. **70** (2001) 2054.

[27] P. Prelovsek, and I. Sega: Phys. Rev. Lett. **93** (2004) 207202.

[28] S. Fujimoto: Phys. Rev. B **63** (2001) 024406.

[29] P. Mendels, J. Bobroff, G. Collin, H. Alloul, M. Gabay, J.F. Marucco, N. Blanchard and B. Grenier: Europhys. Lett. **46** (1999) 678.

[30] K. Ishida, Y. Kitaoka, K. Yamazoe, K. Asayama, and Y. Yamada: Phys. Rev. Lett. **76** (1996) 531.

[31] A. V. Mahajan, H. Alloul, G. Collin, and J. F. Marucco: Phys. Rev. Lett. **72** (1994) 3100.

[32] W. A. MacFarlane, J. Bobroff, H. Alloul, P. Mendels, N. Blanchard, G. Collin, and J.-F. Marucco: Phys. Rev. Lett. **85** (2000) 1108.

[33] A. V. Mahajan, H. Alloul, G. Collin, J. F. Marucco, G. Collin, and J.-F. Marucco: Eur. Phys. J. **B** 13 (2000) 457.

[34] J. Bobroff, W. A. MacFarlane, H. Alloul, P. Mendels, N. Blanchard, G. Collin, and J.-F. Marucco: Phys. Rev. Lett. **83** (1999) 4381.

[35] M.-H. Julien, T. Feher, M. Horvatic, C. Berthier, O.N. Bakharev, P. Segransan, G. Collin, J.-F. Marucco: Phys. Rev. Lett. **84** (2000) 3422.

[36] Y. Fukuzumi, K. Mizuhashi, K. Takenaka, and S. Uchida: Phys. Rev. Lett. **76** (1996) 684.

[37] D.Jaccard, E. Vargoz, K. Alami-Yadri, H. Wilhelm: cond-mat/9711089.

[38] J. Flouquet, P. Haen, F. Lapierre, C. Fierz, A. Amato and D. Jaccard: J. Mag. Mag. Matt. **76&77** (1998) 285.

[39] H. Wilhelm, S. Raymond, D. Jaccard, O. Stockert, H.V. Lohneysen and A. Rosch: J. Phys.: Condens. Matter **13** (2001) L329.

[40] Y. Nakajima, K. Izawa, Y. Matsuda, S. Uji, T. Terashima, H. Shishido, R. Settai, Y. Onuki and H. Kontani, J. Phy. Soc. Jpn. **73** (2004) 5.

[41] Y. Nakajima, K. Izawa, Y. Matsuda, K. Behnia, H. Kontani, M. Hedo, Y. Uwatoko, T. Matsumoto, H. Shishido, R. Settai and Y. Onuki: to be published in J. Phy. Soc. Jpn. **75** (2006) 023705.

[42] H. Taniguchi et al.: unpublished.

[43] Y. Ando, G.S. Boebinger, A. Passner, T. Kimura and K. Kishio: Phys. Rev. Lett. **75** (1995) 4662.

[44] G.S. Boebinger, Y. Ando, A. Passner, T. Kimura, M. Okuya, J. Shimoyama, K. Kishio, K. Tamasaku, N. Ichikawa, and S. Uchida: Phys. Rev. Lett. **77** (1996) 5417.

[45] T. Sekitani, M. Naito, and N. Miura: Phys. Rev. B **67** (2003) 174503.

[46] T. Kawakami, T. Shibauchi, Y. Terao, M. Suzuki, and L. Krusin-Elbaum: Phys. Rev. Lett. **95** (2005) 017001.

[47] R.L. Greene: private communication.

[48] S.H. Pan, E.W. Hudson, K.M. Lang, H. Eisaki, S. Uchida and J.C. Davis: Nature **403** (2000) 746.

[49] B. Nachumi, A. Keren, K. Kojima, M. Larkin, G. M. Luke, J. Merrin, O. Tchernyshov, and Y. J. Uemura, N. Ichikawa, M. Goto, and S. Uchida: Phys. Rev. Lett. **77** (1996) 5421.

[50] T. Nakano, N. Momono, T. Nagata, M. Oda and M. Ido: Phys. Rev. B **58** (1998) 5831.

[51] J. Lee, A. Slezak and J.C. Davis: J. Phys. Chem. Solids **66** (2005) 1370.

[52] N. Momono, A. Hashimoto, Y. Kobatake, M. Oda and M. Ido: J. Phys. Soc. Jpn. **74** (2005) 2400.

[53] J. Kanamori: Prog. Theor. Phys. **30** (1963) 275.

[54] B. Holm and F. Aryasetiawan: Phys. Rev. B **56** (1997) 12825.

[55] B. Holm and U. von Barth: Phys. Rev. B **57** (1998) 2108.

[56] P. Garcia-Gonzalez and R.W. Godby: Phys. Rev. B **63** (2001) 075112.

[57] G. M. Eliashberg : Sov. Phys. JETP **14** (1962), 886.

[58] J.S. Langer: Phys. Rev. **120** (1960) 714.

[59] In these equations, we drop the “incoherent part of conductivity σ_{imc} ”, which gives a finite (quantitatively important) contribution at higher temperatures. The expression for σ_{imc} is derived in H. Kontani and H. Kino: Phys. Rev. B **63** (2001) 134524.

[60] T. R. Chien, Z. Z. Wang, and N. P. Ong: Phys. Rev. Lett. **67** (1991) 2088.

[61] present authors: unpublished.

[62] J.S. Langer: Phys. Rev. **121** (1961) 1090.

[63] H. Ikeda, Y. Nishikawa and K. Yamada: J. Phys.: Condens. Matter **15** (2003) S2241.

[64] G. Baym and L.P. Kadanoff: Phys. Rev. **124** (1961), 287; G. Baym: Phys. Rev. **127** (1962), 1391.

[65] J. Schmalian, D. Pines and B. Stojkovic: Phys. Rev. B **60** (1999) 667.

[66] P. Mendels, H. Alloul, J. H. Brewer, G. D. Morris, T. L. Duty, S. Johnston, E. J. Ansaldo, G. Collin, J. F. Marucco, C. Niedermayer, D. R. Noakes and C. E. Stronach: Phys. Rev. B **49** (1994) 10035.

[67] H. Fukuyama, N. Nagaosa, M. Saito and T. Tanimoto: J. Phys. Soc. Jpn. **65** (1996) 2377.

[68] Y. Itoh, T. Machi, N. Watanabe, S. Adachi and N. Koshizuka: J. Phys. Soc. Jpn. **70** (2001) 1881.

[69] K. Kudo and K. Yamada: J. Phys. Soc. Jpn. **73** (2004) 2219.

[70] K. Miyake and O. Narikiyo: J. Phys. Soc. Jpn. **71** (2002) 867.

[71] V. Dobrosavljevic and G. Kotliar: Phys. Rev. B **50** (1994) 1430.

[72] M. Ulmke, V. Janis and D. Vollhardt: Phys. Rev. B **51** (1995) 10411.

[73] T. Mutou: Phys. Rev. B **60** (1999) 2268.